Seismic Design of Partially Post-Tensioned Precast Concrete Walls

Yahya C. Kurama, Ph.D., P.E.
Associate Professor
Department of Civil Engineering and Geological Sciences
University of Notre Dame
Notre Dame, Indiana

This paper proposes a seismic design approach for precast concrete structural walls that use a combination of mild steel and high strength post-tensioning steel reinforcement across horizontal joints for flexural resistance. The mild steel reinforcement is designed to yield in tension and compression, providing inelastic energy dissipation. The post-tensioning steel provides self-centering capability, reducing the residual (i.e., permanent) lateral displacements of the wall due to a large earthquake. The proposed design approach is a performance-based approach that aims to limit the wall lateral displacements to an allowable target displacement. The design approach is critically evaluated based on nonlinear static and nonlinear dynamic time history analyses of two prototype walls. A design example is provided at the end of the paper.

Recent research[1-11] conducted as part of the PRESSS (PREcast Seismic Structural Systems) research program and other research programs has shown that precast concrete wall and frame structures that use a combination of high strength post-tensioning (PT) steel and mild steel reinforcement crossing the joints between the precast members have desirable seismic characteristics. These structures are referred to as partially post-tensioned structures in this paper (also referred to as "hybrid" structures in the literature), where the term "partial post-tensioning" indicates the use of mild steel reinforcement to provide part of the flexural resistance.

As an example, Fig. 1 shows the elevation and cross section (near the base) of a six-story partially post-tensioned precast concrete wall. The desired nonlinear behavior of the wall under lateral loads is governed by the opening of gaps along the horizontal joints between the precast wall panels and between the wall and the foundation.[1]

The PT steel provides a restoring force that closes the gaps upon unloading, resulting in a self-centering capability (i.e., the ability of the structure to return toward its original undisplaced position at the end of an earthquake). The mild steel reinforcement is designed to yield in tension and compression at the wall base, providing inelastic energy dissipation. Both the PT steel and the mild steel reinforcement contribute to the flexural resistance of the structure to resist lateral loads, resulting in an efficient use of all constituent materials.

The PT tendons are placed inside oversize ducts that are not grouted, and are anchored to the wall only at the roof and at the foundation. The use of unbonded tendons allows the wall to go through significant nonlinear lateral displacements without "yielding" the PT steel. The mild steel reinforcing

bars crossing the horizontal joints are also passed through preformed ducts in each wall panel; however, these ducts are grouted to provide adequate anchorage and development to the steel.

In order to prevent fracturing of the mild steel reinforcement, the bond between the mild steel bars and the concrete may be prevented by wrapping the reinforcement over a predetermined height near the horizontal joint at the base of the wall where the largest gap opening occurs. The mild steel reinforcement is extended a sufficient height above the wall base, after which the bars that are no longer needed for flexural resistance may be terminated in a staggered pattern.

In comparison with partially post-tensioned precast concrete frame structures,[6-11] previous research on partially post-tensioned wall structures is limited.[1-5] Kurama[1] conducted an analytical parameter investigation on the nonlinear dynamic behavior of precast concrete walls with different amounts of post-tensioning steel and mild steel reinforcement. It was shown that the lateral displacements of post-tensioned precast walls under earthquakes can be considerably reduced by using mild steel reinforcement crossing the horizontal joints.

Based on the previous investigation by Kurama,[1] this paper introduces a seismic design approach that aims to limit the lateral displacements of a partially post-tensioned wall to an allowable target displacement. Guidelines for the selection of the amount of PT steel and mild steel reinforcement, as well as the amount of concrete confinement needed, to achieve the design performance objectives are provided.

The proposed design approach is critically evaluated based on nonlinear static monotonic and reversed cyclic lateral load analyses and nonlinear dynamic time history analyses of two prototype walls. The conditions for which the design approach appears to be valid and the conditions for which improvement is needed are discussed. A design example is provided in Appendix B.

The draft ACI ITG T5.1 document, "Acceptance Criteria for Special Precast Concrete Structural Walls Based on Validation Testing and Commentary,"[12,13] defines the minimum experimental evidence needed to validate the use of precast concrete walls in seismic regions of the United States. One of the requirements of ACI ITG T5.1 is that, prior to testing, a design procedure be developed and used to proportion the test specimens. The proposed design approach may serve this purpose.

Extensive experimental and analytical investigations on partially post-tensioned precast concrete frames have led to the successful development[14-17] and application[18] of guidelines for the use of these structures in seismic regions. Ultimately, the design recommendations provided in this paper may be useful in the development of similar seismic design guidelines for partially post-tensioned wall structures.

THE PROTOTYPE WALLS

This paper is based on two prototype partially post-tensioned precast concrete walls, each six stories in height. The walls are referred to as Wall PP6-BO and Wall PP6-EO and were designed for a site with a "stiff" soil profile (Site Class D in IBC-2003[19]) in Los Angeles, California (to represent a region with high seismicity). The elevation and cross section

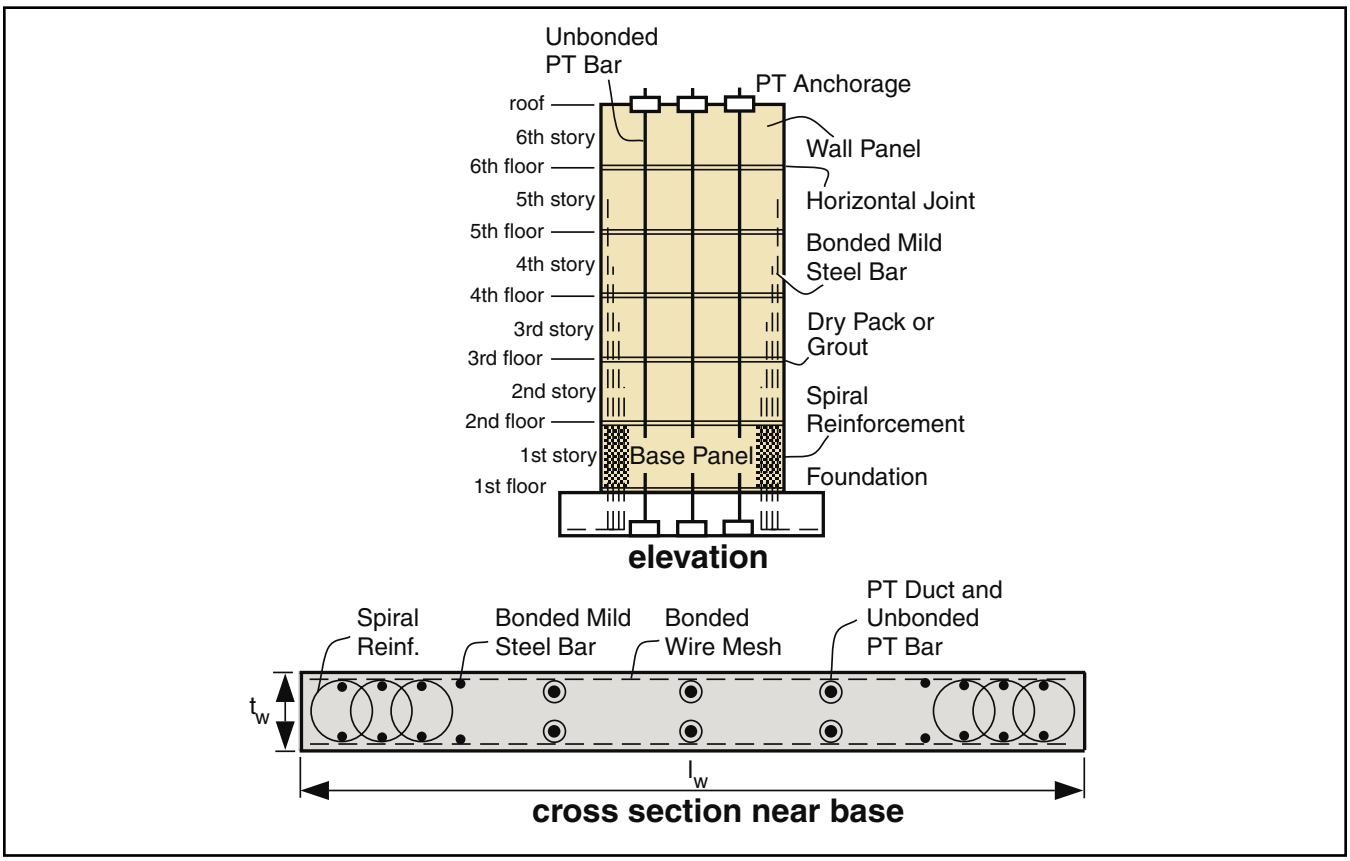

Fig. 1. Partially post-tensioned precast concrete wall.

(near the base) views of the walls and the plan views of the buildings for which the walls were designed are shown in Figs. 2 and 3, respectively.

It is assumed that the walls provide the entire lateral load resistance in the north-south direction of the buildings and that the walls in each building are identical. The lateral load resisting frames in the east-west direction are not addressed in the paper.

High strength bars are used as PT tendons over the height of the prototype walls. The total areas of the PT steel and mild steel reinforcement as a percentage of the gross cross section area of the walls (referred to as the PT steel ratio, ϱ_p, and mild steel ratio, ϱ_s) are given in Table 1. All of the mild steel reinforcement is placed at a spacing of 2.5 in. (63 mm) at the wall boundaries near each end. The mild steel bars are terminated at staggered heights above the base of the wall; however, this is not investigated in the paper.

Dry-pack or grout is used between the wall panels for construction tolerances and for alignment purposes (see Fig. 1). As shown in Fig. 2, circular spiral reinforcement is used in the base panel to confine the concrete near the corners of each wall at the base. Note that closed rectangular hoops may also be used instead of circular spirals. The spiral confinement ratios for the walls, ϱ_{sp} (defined as the ratio of the volume of spiral reinforcement to the volume of confined concrete core), are given in Table 1.

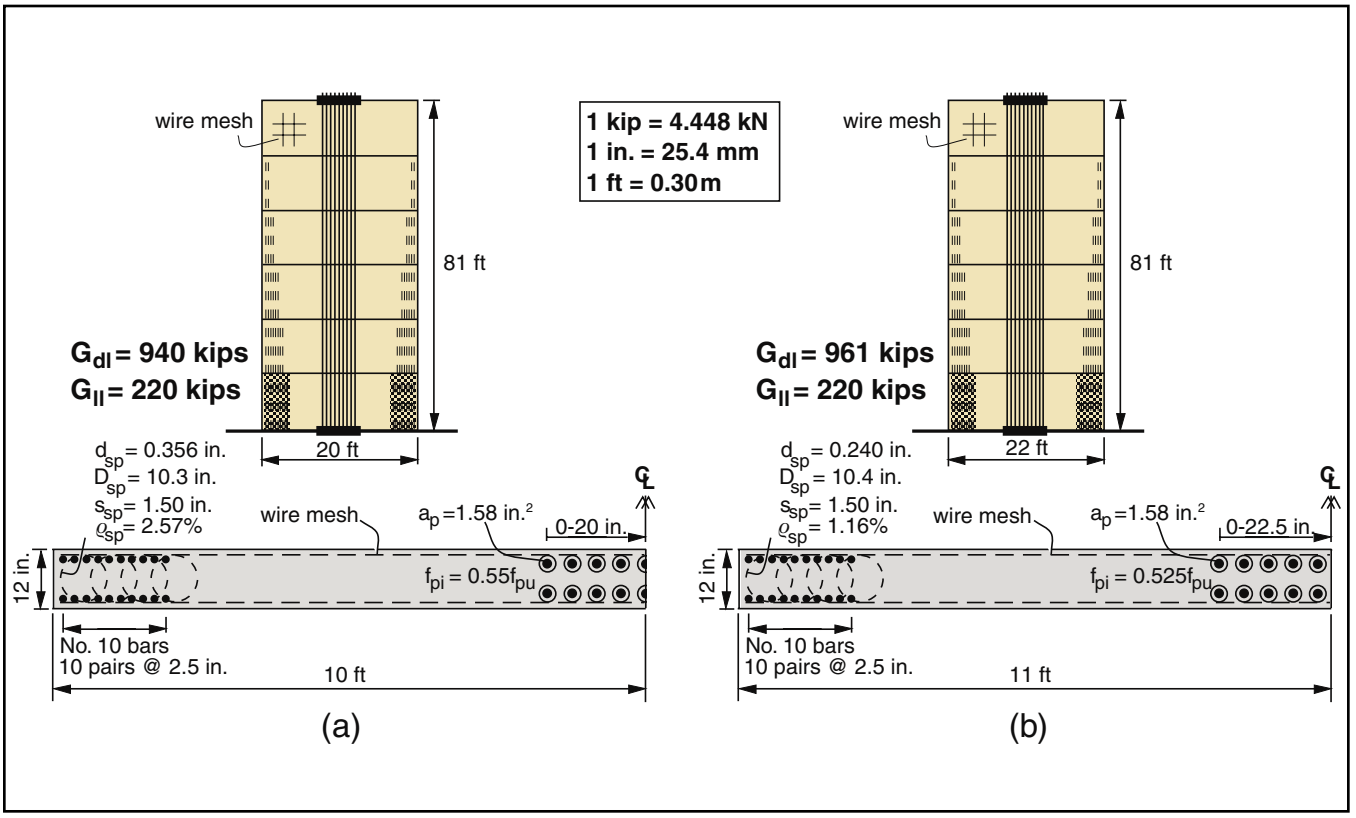

Fig. 2. Prototype walls: (a) Wall PP6-BO; (b) Wall PP6-EO.

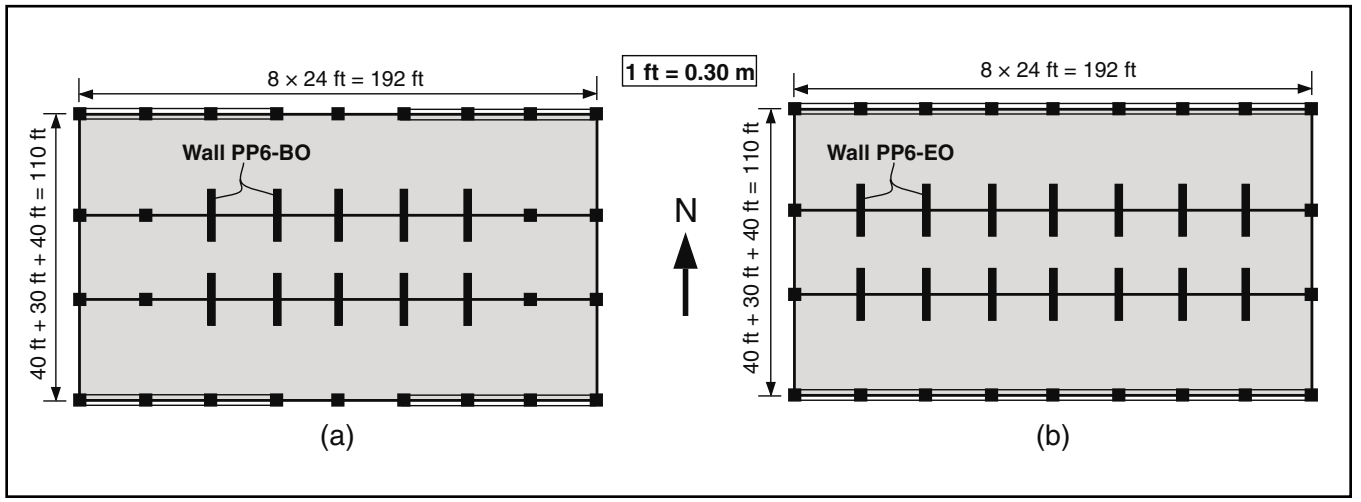

Fig. 3. Plan view of prototype buildings: (a) Building PP6-BO; (b) Building PP6-EO.

A nominal amount of wire mesh is used as additional bonded steel reinforcement in the wall panels. The wire mesh reinforcement is not continuous across the horizontal joints and, thus, does not contribute to the flexural strength of the wall.

The assumed idealized multilinear design/analysis properties of the mild steel, PT steel, and concrete are shown in Fig. 4. The stress-strain relationship for the mild steel [Fig. 4(a)] is based on typical experimental results reported by Paulay and Priestley.[20]

The yield strength and ultimate (peak) strength of the mild steel are assumed to be equal to f_{sy} = 60 ksi (414 MPa) and f_{su} = 97 ksi (669 MPa), respectively, with the ultimate strength reached at a strain of 0.06. Similarly, the "yield" (i.e., linear limit) strength and ultimate (peak) strength of the PT steel are assumed to be equal to f_{py} = 120 ksi (827 MPa) and f_{pu} = 160 ksi (1103 MPa), respectively, with the ultimate strength reached at a strain of 0.0351 [Fig. 4(b)].

The assumed Young's modulus of the mild steel and PT steel is equal to $E_s = E_p$ = 29,000 ksi (199955 MPa), and that of the concrete is equal to $E_c = 57{,}000(f_c')^{0.5}$ (in psi). The compressive strength of the unconfined concrete is assumed to be f_c' = 6 ksi (41.4 MPa), reached at a strain of ε_0 = 0.002, with the ultimate (i.e., crushing) strain reached at ε_u = 0.004. The stress-strain relationships of the unconfined concrete [Fig. 4(c)] and the spiral confined concrete are based on a model developed by Mander et al.[21] The small amount of

Table 1. Prototype walls.

Wall	No. of walls	$l_w \times t_w$ (in. × in.)	ϱ_p (percent)	ϱ_s (percent)	ϱ_{sp} (percent)	T_{e1} (sec.)
PP6-BO	10	240 × 12	0.99	1.76	2.57	0.57
PP6-EO	14	264 × 12	1.00	1.60	1.16	0.43

Note: 1 in. = 25.4 mm.

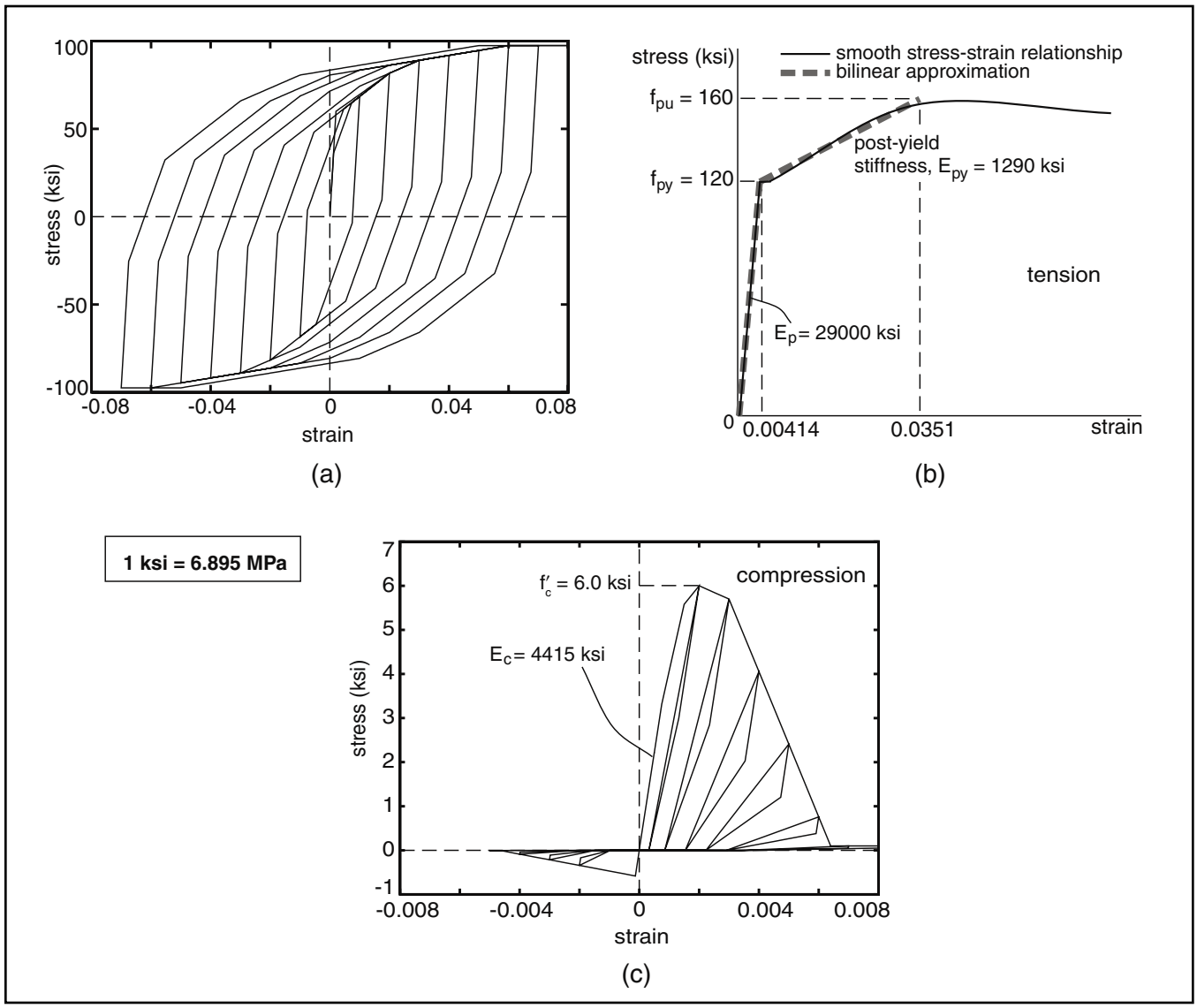

Fig. 4. Design/analysis material properties: (a) mild reinforcing steel; (b) post-tensioning steel; (c) unconfined concrete.

concrete confinement provided by the wire mesh used in the wall panels is ignored.

The cumulative (from the upper stories) axial forces at the bases of the prototype walls, G_{dl} and G_{ll}, due to the unfactored design dead loads and the unfactored unreduced design live loads, respectively, are shown in Fig. 2. The walls were designed under a hypothetical load condition of 100 percent of unfactored design dead loads plus 25 percent of unfactored unreduced design live loads (to represent the amount of gravity load that may be acting on each wall during an earthquake), combined with earthquake-induced lateral loads. No capacity reduction factors were used in the design of the walls.

The analytical evaluation of the seismic response of the prototype walls was also conducted under this hypothetical load condition. Note that code specified (e.g., IBC-2003[19]) capacity reduction factors and load combinations would need to be used in practice; however, this is not done in the paper to facilitate direct comparisons between the design estimations and the analysis results.

Wall PP6-BO was designed not to exceed (on average) a target allowable peak roof drift of Δ_t = 2.4 percent under a survival level earthquake (referred to as the Maximum Considered Earthquake in IBC-2003[19]), where the roof drift is defined as the roof lateral displacement divided by the wall height. Yielding of the PT steel is allowed to occur at this peak displacement level; however, crushing of the confined concrete is prevented in order to achieve a "basic performance objective" of collapse prevention.

In comparison, Wall PP6-EO was designed for a smaller, more strict target allowable peak roof drift of Δ_t = 1.2 percent under the same survival level earthquake. Both the crushing of the confined concrete and the yielding of the PT steel are prevented at this displacement level, corresponding to an "enhanced performance objective." More details on the design of the prototype walls are provided in Appendix B, with the procedure used in their design described below.

PROPOSED DESIGN APPROACH

The proposed design approach consists of eight components: (1) seismic design objectives; (2) wall design base moment demand, M_{wd}; (3) area of PT steel reinforcement, A_p, and mild steel reinforcement, A_s; (4) concrete confinement; (5) detailing of mild steel reinforcement; (6) yielding of PT steel reinforcement; (7) shear design; and (8) stability of wall panels.

Each of these design components is described below. Note that an experimental validation is needed before the proposed design approach can be used in practice.

Seismic Design Objectives

The proposed design approach requires the selection of one or more seismic design objectives. Each seismic design objective includes the following:

1. A seismic demand level, for example:
   - Design demand level (probability of exceedence of 10 percent in 50 years);
   - Survival demand level (probability of exceedence of 2 percent in 50 years).
2. An allowable target peak roof drift demand, Δ_t.
3. A seismic performance level and corresponding structure limit state, for example:
   - Basic performance objective to prevent crushing of the confined concrete;
   - Enhanced performance objective to prevent yielding of the PT steel in addition to crushing of the confined concrete.

Wall Design Base Moment Demand, M_{wd}

The determination of the wall design base moment demand, M_{wd}, requires that trial values be selected for the number, n_w, and gross dimensions (length, l_w, and thickness, t_w) of the walls in a building. Then, a linear-elastic modal analysis of the structure is conducted to determine the first (i.e., fundamental) mode shape, $\{\phi_{e1}\}$, and period, T_{e1}.

Alternatively, $\{\phi_{e1}\}$ and T_{e1} can be estimated using approximate procedures (e.g., as described in the Equivalent Lateral Force procedure of IBC-2003[19]). It is assumed that the displacement response of the structure is controlled by the first mode, and that the shape of this mode remains essentially constant throughout the response history.

The wall design base moment demand, M_{wd}, and base shear demand, V_{wd}, are determined by distributing the structure design base shear demand, V_{sd}, to the lateral load resisting members in the plan and over the height of the structure as described in the Equivalent Lateral Force Procedure of IBC-2003.[19] The structure design base shear demand, V_{sd}, corresponding to each seismic design objective is calculated as:

$$V_{sd} = \frac{M_{e1} f_\xi S}{R_1} \tag{1}$$

where

M_{e1} = L^2/M^* = design effective linear-elastic first mode mass of the structure

f_ξ = damping adjustment coefficient

S = site adjusted linear-elastic design spectral response acceleration (based on T_{e1}) for the site condition and seismic demand level used in design (e.g., as determined from IBC-2003[19])

R_1 = strength ratio based on an equivalent single-degree-of-freedom (SDOF) system used to represent the nonlinear dynamic lateral displacement response of the structure

The quantity $L = \{\phi_{e1}\}^T[M]\{1\}$ is referred to as the earthquake excitation factor and $M^* = \{\phi_{e1}\}^T[M]\{\phi_{e1}\}$ is the generalized mass for the first mode,[22-25] where $[M]$ is the design diagonal mass matrix assigned to the structure. It is assumed that the structure mass is distributed equally between the walls in the building through a "rigid" diaphragm.

The damping adjustment coefficient, f_ξ, accounts for the difference (if any) in the assumed viscous damping ratio, ξ, for the structure being designed and the viscous damping ratio corresponding to the S/R_1 value used in design. For example, a value of ξ = 3 percent is assumed for the prototype structures in this paper, whereas a value of ξ_0 = 5 percent is used in IBC-2003.[19] The damping adjustment coefficient accounts for the difference between ξ and ξ_0, and can be calculated as:[26]

$$f_\xi = \frac{(1 + 25\xi_0)^{0.5}}{(1 + 25\xi)^{0.5}} \quad (2)$$

For $\xi_0 = 5$ percent and $\xi = 3$ percent, f_ξ is equal to 1.13. Note that this value is similar to the damping adjustment coefficients given in the FEMA 356 document, "Prestandard and Commentary for the Seismic Rehabilitation of Buildings."[27]

The strength ratio, R_1, is used to determine the required structure base shear strength, V_{sd}, to limit (on average) the peak roof drift demand to the allowable target roof drift, Δ_t. An equivalent nonlinear SDOF system, referred to as the BP system, is used to determine the strength ratio, R_1, based on the following relationship:

$$R_1 = [c(\mu_t - 1) + 1]^{1/c} \quad (3)$$

with

$$c = \frac{T_{e1}^a}{T_{e1}^a + 1} + \frac{b}{T_{e1}} \quad (4)$$

where μ_t is the displacement ductility demand corresponding to Δ_t, and a and b are regression coefficients based on SDOF nonlinear dynamic time history analyses using the equivalent system. The form of the relationship in Eqs. (3) and (4) was developed by Nassar and Krawinkler.[28]

More details on the equivalent SDOF BP system, which is used to estimate the seismic displacement response of the prototype walls in this paper, are given later. Table 2 shows the a and b regression coefficients for the BP system and selected seismic design conditions (site seismicity, demand level, and site soil type) determined as described in Farrow and Kurama.[29,30]

The wall design base moment demand, M_{wd}, and base shear demand, V_{wd}, for each seismic design objective are determined using an iterative procedure as follows:

1. Assume a value for the ductility demand, μ_t, corresponding to Δ_t.
2. Calculate R_1 from Eqs. (3) and (4).
3. Calculate V_{sd} from Eq. (1).
4. Calculate V_{wd} by distributing V_{sd} vertically over the height and horizontally to the lateral load resisting members in the plan of the structure.
5. Estimate the peak roof drift demand, Δ_d, as:

$$\Delta_d = \mu_t \frac{V_{wd}}{K_{wi} h_w} \quad (5)$$

where K_{wi} is the wall linear-elastic lateral stiffness and h_w is the wall height.

6. Check if Δ_d from Step 5 is sufficiently close to the allowable target roof drift Δ_t. Repeat Steps 1 to 5 if Δ_t is exceeded or if Δ_d is significantly smaller than Δ_t (indicating an overdesign). If the desired design conditions cannot be achieved, the trial wall length, l_w, and/or number of walls, n_w, in the structure may need to be revised.
7. Calculate M_{wd} from the distribution of V_{wd} over the height of the wall.

Flexural Steel Areas

In order to determine the flexural steel areas needed, the nominal base moment strength of a partially post-tensioned wall is divided into three components, M_{ws}, M_{wp}, and M_{wn}, representing the contributions of the wall mild steel reinforcement, PT steel reinforcement, and applied (external) wall design axial load, respectively, to satisfy the design base moment demand, M_{wd}. Thus:

$$M_{wd} = M_{ws} + M_{wp} + M_{wn} \quad (6)$$

Using the equilibrium of the forces in Fig. 5 at the wall base, Eq. (6) can be written as:

$$M_{wd} = A_s f_s \left(d_{sc} - \frac{l_w}{2}\right) + A'_s f'_s \left(\frac{l_w}{2} - d'_{sc}\right) + \frac{C(l_w - a_c)}{2} \quad (7)$$

$$C = 0.85 f'_c a_c t_w = A_s f_s - A'_s f'_s + A_p f_{pi} + N_{wd} \quad (8)$$

where

C = total compressive stress resultant at wall base
f'_c = compressive strength of unconfined concrete
a_c = length of assumed uniform (i.e., rectangular) stress block at wall base
t_w = wall thickness
l_w = wall length
N_{wd} = applied (external) wall design axial force at base

Table 2. Regression coefficients a and b for BP system.

Hysteresis type	Site seismicity	Demand level	Site soil type	Regression coefficient	
				a	b
BP (β_r = 1/3)	Los Angeles, CA	Design	D	3.82	0.87
			E	0.65	1.02
		Survival	D	1.08	0.89
	Seattle, WA	Design	D	2.39	0.64
			E	0.61	0.68
		Survival	D	1.33	0.63
	Boston, MA	Design	D	0.92	0.61
			E	0.43	0.59
		Survival	D	0.93	0.62

A_p = total PT steel area
f_{pi} = design initial stress in PT steel after losses (ignoring any changes in the PT steel stresses due to the lateral displacements of the wall)
A'_s = total area of mild steel reinforcement on compression side of wall
A_s = total area of mild steel reinforcement on tension side of wall
f'_s = stress of mild steel reinforcement at centroid of A'_s
f_s = stress of mild steel reinforcement at centroid of A_s
d'_{sc} = distance from compression end of wall to centroid of A'_s
d_{sc} = distance from compression end of wall to centroid of A_s

Assuming that $A'_s = A_s$ and $d'_{sc} = l_w - d_{sc}$ (i.e., symmetric placement of reinforcement about the wall centerline), and $f'_s = f_s = f_{sy}$ (i.e., both the compression steel and the tension steel have yielded) in Eqs. (7) and (8), the wall nominal "yield" moment strength M_{wy} to satisfy the design base moment demand M_{wd} can be written as:

$$M_{wd} = M_{wy} = A_s f_{sy}(l_w - 2d'_{sc}) + \frac{A_p f_{pi}(l_w - a_c)}{2} + \frac{N_{wd}(l_w - a_c)}{2} \quad (9)$$

where the three terms on the right hand side of Eq. (9) correspond to M_{ws}, M_{wp}, and M_{wn}, respectively, contributing to the wall yield moment strength M_{wy}.

In order to determine the required steel areas, a new parameter β_m, referred to as the mild steel moment ratio, is defined as $\beta_m = M_{ws}/(M_{wp} + M_{wn})$. Then, using Eq. (6), it can be shown that:

$$M_{ws} = \frac{M_{wd}\beta_m}{\beta_m + 1} \quad \text{and} \quad M_{wp} = \frac{M_{wd}}{\beta_m + 1} - M_{wn} \quad (10)$$

The β_m value is a measure of the relative amounts of mild steel and PT steel reinforcement used in a wall. Designs using larger β_m result in walls with larger amounts of mild steel reinforcement. If the mild steel contribution is too small (i.e., the β_m value is too small), then the inelastic energy dissipation of the system may be very small.

Conversely, if the PT steel contribution is too small (i.e., the β_m value is too large), then the self-centering capability of the wall may be very small, and thus, it may not be possible to yield the mild steel reinforcement in compression and close the gaps at the horizontal joints. In order to determine M_{ws} and M_{wp} from Eq. (10), a β_m value needs to be assumed for the trial structure. A value of $0.75 \le \beta_m \le 1$ is recommended for design. Both of the prototype structures investigated in this paper were designed with $\beta_m = 1.0$.

Once the mild steel and PT steel contributions, M_{ws} and M_{wp}, to satisfy the wall design base moment demand, M_{wd}, are determined as described above, the next step is to estimate the required steel areas.

Post-Tensioning Steel Area, A_p—Combining Eqs. (9) and (10), the PT steel contribution to the total wall base moment resistance can be determined as follows:

$$M_{wp} = \frac{M_{wd}}{\beta_m + 1} - \frac{N_{wd}(l_w - a_c)}{2} = \frac{A_p f_{pi}(l_w - a_c)}{2} \quad (11)$$

Then:

$$A_p = \frac{2M_{wd}}{(\beta_m + 1)(l_w - a_c) f_{pi}} - \frac{N_{wd}}{f_{pi}} \quad (12)$$

where

$$a_c = \frac{N_{wd} + A_p f_{pi}}{0.85 f'_c t_w} \quad (13)$$

The calculation of A_p using Eq. (12) requires an iterative solution based on an assumed length, a_c, for the concrete compression stress block. Eqs. (12) and (13) are repeated until satisfactory agreement in the value of a_c is obtained.

Mild Steel Area, A_s—Similarly, the mild steel contribution to the total wall base moment resistance can be determined as follows:

$$M_{ws} = \frac{M_{wd}\beta_m}{\beta_m + 1} = A_s f_{sy}(l_w - 2d'_{sc}) \quad (14)$$

from which

$$A_s = \frac{M_{wd}\beta_m}{(\beta_m + 1)(l_w - 2d'_{sc}) f_{sy}} \quad (15)$$

The calculation of A_s using Eq. (15) requires an iterative solution based on an assumed value of d'_{sc}, which is then compared with the d'_{sc} value from the placement of the mild steel reinforcing bars in the wall cross section.

Once the mild steel bars are selected and placed in the cross section, the strains in the bars are calculated assuming a linear strain diagram (i.e., plane sections remain plane) and a neutral axis depth of $c_c = a_c/\beta_1$, where β_1 is a concrete rectangular stress block parameter as described in ACI 318.[31] If the calculated mild steel bar strains are smaller than the yield strain, then the determination of A_s above may need to be revised using a modified form of Eq. (9).

Concrete Confinement

Concrete confinement is needed at the wall boundaries to prevent premature crushing and failure of the concrete before the peak roof drift demand, Δ_d, is reached. For this purpose, the required uniaxial compressive strain capacity of the confined concrete, ε_{cu}, is determined as:

$$\varepsilon_{cu} = c_{cu}\phi_{cu} \quad (16)$$

where

c_{cu} = neutral axis depth
ϕ_{cu} = estimated curvature at wall base

Ignoring the thickness of the unconfined cover concrete, the neutral axis depth is estimated as:

$$c_{cu} = \frac{N_{wd} + A_p f_{py}}{0.85 f'_{cc} t_w} \quad (17)$$

Note that a more accurate estimate for c_{cu} can be obtained by using the confined concrete thickness instead of the entire thickness, t_w, of the wall. In Eq. (17), f'_{cc} is the ultimate (i.e.,

peak) strength of the confined concrete and f_{py} is the yield strength of the PT steel. It is assumed that all of the PT tendons in the cross section are at the yield stress.

The curvature, ϕ_{cu}, is estimated by assuming that the wall lateral displacements occur as a result of a concentrated rotation at the wall base and that the flexural deformations are uniformly distributed over a "plastic hinge height" as:

$$\phi_{cu} = \frac{\Delta_d}{h_{wp}} = \frac{\Delta_d}{0.2l_w} \quad (18)$$

where $h_{wp} = 0.2l_w$ is the assumed plastic hinge height as determined from the lateral load analyses of the walls described in this paper and in Kurama.[1] An experimental validation of Eqs. (16) to (18) is needed before these equations can be used in practice.

Note that the determination of the required compressive strain capacity of the confined concrete, ε_{cu}, based on Eqs. (16) to (18), is an iterative process since the strength of the confined concrete, f'_{cc}, in Eq. (17) is not known in advance. A confinement model, such as that described by Mander et al.,[21] is used to develop the stress-strain relationship of the confined concrete and to determine the amount and details of the confinement reinforcement needed to achieve the strain capacity, ε_{cu}.

The confinement reinforcement should extend over a length, l_c, and height, h_c, near both ends of the wall at the base where the concrete strains are greater than or equal to the assumed crushing strain of the unconfined concrete, ε_u.

A linear strain diagram defined by c_{cu} and ϕ_{cu} from Eqs. (17) and (18) may be used to determine the confined wall length at each end as:

$$l_c = c_{cu}\left(1 - \frac{\varepsilon_u}{\varepsilon_{cu}}\right) \quad (19)$$

The determination of the confined wall height, h_c, depends on the bending moment diagram over the wall height and is not within the scope of this paper.

Detailing of Mild Steel Reinforcement

Fracture and low cycle fatigue failure of the mild steel reinforcement at the wall base should be prevented. For this purpose, a linear strain diagram defined by c_{cu} and ϕ_{cu} from Eqs. (17) and (18) can be used to estimate the maximum strain in the mild steel bar on the extreme tension side of the wall. If necessary, the strains in the mild steel reinforcement can be reduced by placing the bars closer to the wall centerline (which may require a redesign) and/or by wrapping the bars to prevent bond over a predetermined height above the base-panel-to-foundation joint. Determination of the wrapped length of mild steel reinforcement is not discussed in this paper.

The mild steel reinforcement should be properly anchored to the foundation and should be extended to a sufficient height above the base of the wall to allow for the development of the ultimate (i.e., peak) strength of the steel in tension and compression at the base-panel-to-foundation joint. The bars that are no longer needed for flexural resistance may be terminated (i.e., cut off) in a staggered pattern over the wall height.

Note that the termination of the mild steel reinforcement over the height of a wall results in a reduction in the flexural strength of the wall cross section where the bars are cut off. This may lead to undesirable behavior due to the opening of larger gaps at the upper floor joints of the wall than the gap along the base-panel-to-foundation joint, even though the design moment is expected to decrease from the bottom (i.e., base) to the top of the wall. Thus, the bar termination points should be carefully determined to achieve a reasonable curtailment pattern over the wall height. The detailing of the mild steel reinforcement over the wall height is not addressed further in this paper.

Yielding of Post-Tensioning Steel Reinforcement

If the design performance objective aims to prevent the yielding of the PT steel (i.e., enhanced objective), a check needs to be conducted to ensure that:

$$\Delta_{py} \geq \Delta_d \quad (20)$$

where Δ_{py} is the wall roof drift corresponding to the yielding of the PT steel estimated as:

$$\Delta_{py} = \frac{u_{py}}{d_{py} - c_{py}} \quad (21)$$

with

$$u_{py} = \frac{f_{py} - f_{pi}}{E_p} l_{pu} \quad (22)$$

In Eqs. (21) and (22):

u_{py} = additional elongation of PT steel from f_{pi} to f_{py}
d_{py} = distance of PT tendon with the largest strain from the compression end of wall
f_{py} = yield strength of PT steel
f_{pi} = initial stress (after losses) of PT steel
l_{pu} = unbonded length of PT steel (assumed to be equal to the wall height)
c_{py} = neutral axis depth at wall base corresponding to yielding of PT steel

It may be assumed that $c_{py} = c_{cu}$ from Eq. (17).

If the yielding of the PT steel needs to be delayed, a lower value of f_{pi} should be used in Eqs. (12) and (13), and the design repeated, or the tendons should be placed closer to the wall centerline. Note that while the results obtained using Eqs. (21) and (22) have been compared with results from the lateral load analyses of the walls described in this paper and in Kurama,[1] an experimental validation of these equations is needed before they can be used in practice.

Shear Design

Shear design of a wall includes design to prevent diagonal tension failure in the wall panels, shear slip failure along the horizontal joints, and failure along the bottom and top edges of the wall panels (especially the base panel) due to a gap opening. The effects of higher modes of vibration[32-38] should be included in determining the wall peak shear force demand, $V_{w,max}$.

Diagonal Tension Failure—Pending experimental validation, ACI 318[31] diagonal tension requirements for prestressed concrete members may be used for the design of partially

post-tensioned precast concrete walls.

Shear Slip Failure—The nominal shear slip strength of a partially post-tensioned wall can be determined as:

$$V_{ss} = \mu_s [(A_s + A'_s) f_{sy} + A_p f_p + N_{wd}] \quad (23)$$

where

μ_s = design coefficient of friction
A_p = area of PT steel
f_p = stress of PT steel

An experimental validation of Eq. (23) needs to be conducted before use in practice. Yielding of the PT steel (if allowed to occur) and subsequent loss in prestress under cyclic loading should be considered in the determination of f_p. If yielding of the PT steel is not allowed to occur (i.e., enhanced performance objective), then $f_p = f_{pi}$ may be assumed. Further information on the design of a fully post-tensioned precast concrete wall to prevent shear slip along the horizontal joints can be found in Kurama et al.[36-38]

Failure Along Panel Bottom/Top Edges—Failure due to uncontrolled cracking along the bottom and top edges of the wall panels (especially the base panel) as a result of a gap opening at the horizontal joints should be prevented. More information on this critical failure mode can be found in Allen and Kurama.[39]

Stability of Wall Panels

Design for the stability of the wall panels includes design to prevent out-of-plane buckling of the wall panels between lateral restraints (usually at the floor and roof levels) and design to prevent buckling of the compression zone in the base panel. In the absence of experimental results, no further information is provided in the paper on this topic.

BEHAVIOR OF PROTOTYPE WALLS UNDER LATERAL LOADING

Fig. 6(a) shows the expected base shear force versus roof drift (V-Δ) behaviors of the prototype Walls PP6-BO and PP6-EO under combined gravity loads and lateral loads. An analytical wall model based on fiber beam-column elements (described in Kurama[1]) was used to conduct the analyses.

Similar to the load condition used in design, the gravity loads acting on each wall were assumed to be equal to $1.00DL + 0.25LL$ (where DL and LL are the unfactored design dead load and the unfactored unreduced design live load, respectively) to represent the amount of gravity load that may be acting on the wall during an earthquake. The distribution of the lateral forces over the height of the walls was assumed to be the same as the distribution of inertial forces corresponding to the fundamental mode of vibration from a linear-elastic modal analysis of each structure.

The three markers in Fig. 6(a) identify the limit states used in the design of Walls PP6-BO and PP6-EO as follows:

1. The ○ marker identifies the yielding of the mild steel reinforcement at the centroid of the bar group on the tension side of the wall;
2. The □ marker identifies the point at which the strain in the extreme post-tensioning tendon reaches the limit of proportionality (note that this limit state is prevented in Wall PP6-EO); and
3. The ◊ marker identifies the axial-flexural failure of the wall as a result of crushing of the spiral confined concrete at the base.

The walls satisfy all of the design requirements. A detailed investigation and comparisons between the estimated design

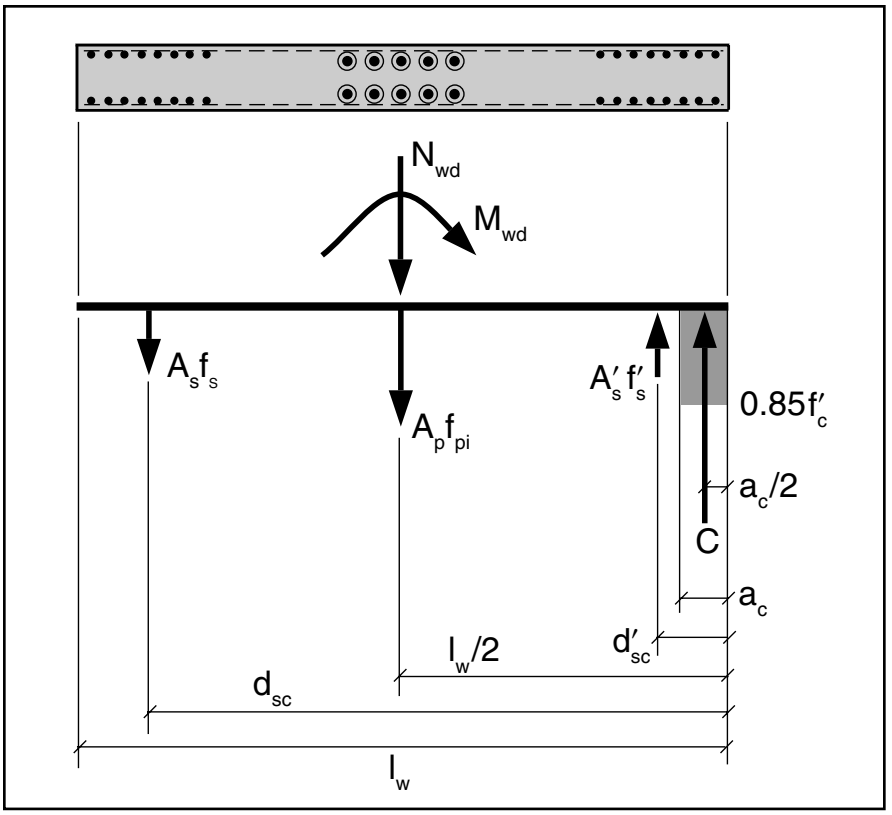

Fig. 5. Equilibrium of forces at the base of a partially post-tensioned wall.

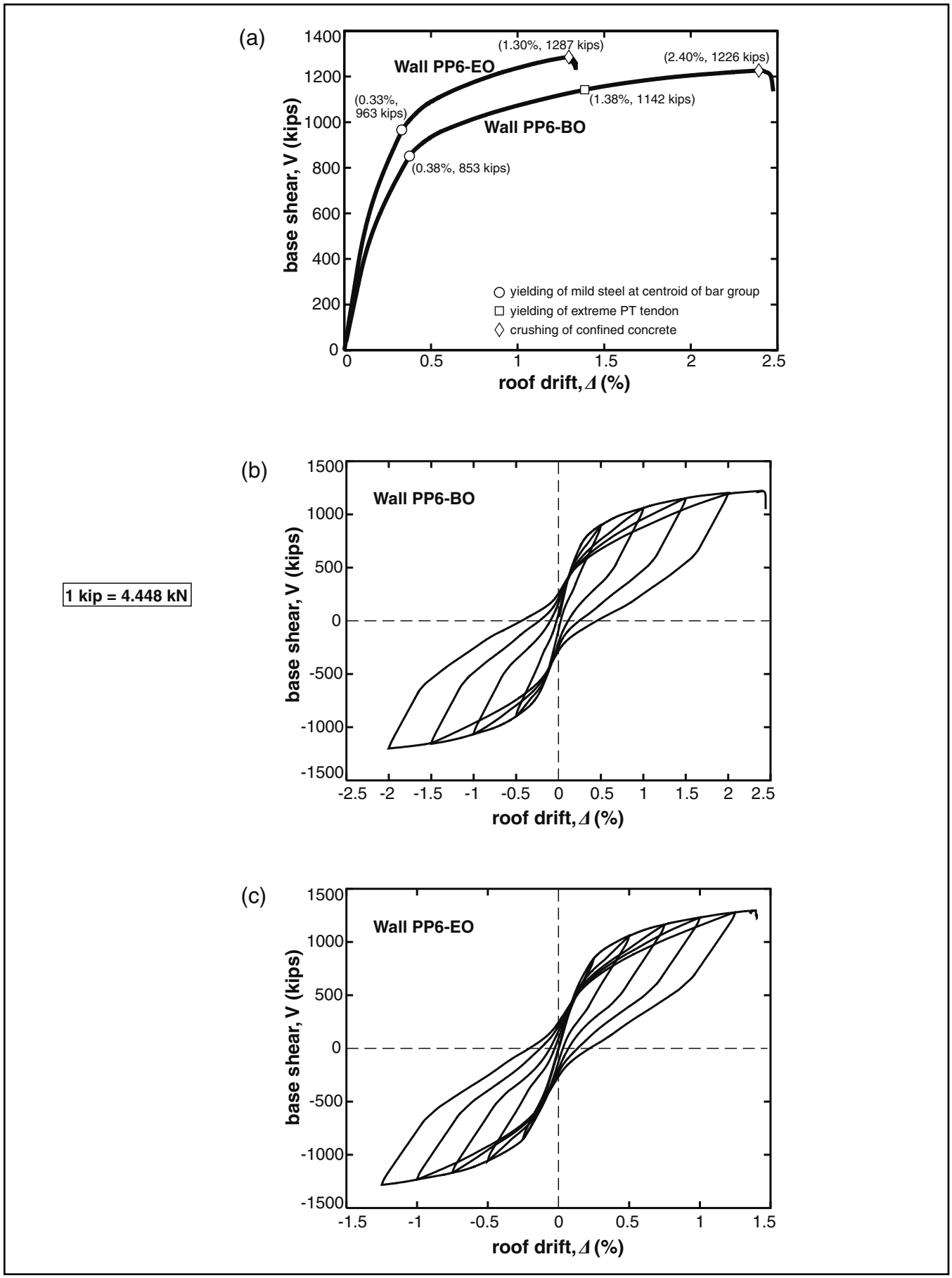

Fig. 6. Behavior of the prototype walls under lateral loading: (a) monotonic loading; (b) cyclic loading, Wall PP6-BO; (c) cyclic loading, Wall PP6-EO.

capacities and demands for Wall PP6-BO are provided in Appendix B.

Figs. 6(b) and 6(c) show the behaviors of Walls PP6-BO and PP6-EO under reversed cyclic loading. Both walls demonstrate stable behavior with considerable inelastic energy dissipation and self-centering capability. The lateral load behavior of a series of walls with varying amounts of mild steel and PT steel reinforcement, similar to the prototype walls in this paper, can be found in Kurama.[1]

The results from the cyclic analyses of Walls PP6-BO and PP6-EO are evaluated for conformance to the ACI ITG T5.1 draft document, "Acceptance Criteria for Special Precast Concrete Structural Walls Based on Validation Testing and Commentary."[12,13] According to ACI ITG T5.1, the relative energy dissipation ratio, β, of a wall should be greater than or equal to 0.125.

The relative energy dissipation ratio is defined for a V-Δ cycle as the ratio of the area D_h enclosed by the hysteresis loop for that cycle to the area of the circumscribing parallelogram. The circumscribing parallelogram area is defined by the initial positive and negative stiffnesses during the first linear-elastic cycle of loading and the peak positive and negative base shear resistances during the cycle for which the relative energy dissipation ratio is calculated.[12,13]

The relative energy dissipation ratio, β, is a measure of the amount of viscous damping in an equivalent linear-elastic system that would result in a similar amount of energy dissipation as the nonlinear system. The ACI ITG T5.1 document[12,13] recommends that if β is smaller than 0.125, there may be inadequate damping for the structure as a whole, and the oscillations of the structure may continue for some time after an earthquake, possibly leading to low-cycle fatigue effects and excessive displacements.

Fig. 7 shows the relative energy dissipation ratio, β, of Walls PP6-BO and PP6-EO based on the cyclic V-Δ behaviors in Figs. 6(b) and 6(c). The horizontal axes show the maximum/minimum roof drift reached during each loading cycle, Δ_c. Wall PP6-BO was displaced to roof drift values of $\pm\Delta_c = \pm 0.5$, 1.0, 1.5, and 2.0 percent during each cycle and Wall PP6-EO was displaced to roof drift values of $\pm\Delta_c = \pm 0.25$, 0.5, 0.75, 1.0, and 1.25 percent [see Figs. 6(b) and 6(c)].

It can be seen from Fig. 7 that the prototype Walls PP6-BO and PP6-EO have similar β values and that β increases as the wall roof drift increases. The shaded regions show the roof drift cycles for which $\beta \geq 0.125$. The results indicate that the walls satisfy the energy dissipation requirement of ACI ITG T5.1 for, approximately, $\Delta_c > 0.3$ percent. As would be expected, only limited (if any) yielding of the mild steel reinforcement occurs at displacements smaller than $\Delta_c \approx 0.3$ percent, resulting in a small amount of inelastic energy dissipation (i.e., the wall behavior is close to linear-elastic).

BEHAVIOR OF WALLS UNDER EARTHQUAKE LOADING

This section investigates the nonlinear dynamic behavior of Walls PP6-BO and PP6-EO under earthquake loading. The ground motions used in the investigation are described first, followed by the equivalent SDOF BP system used for design purposes. Finally, the seismic response of the prototype walls is critically examined based on multi-degree-of-freedom nonlinear dynamic time history analyses.

The nonlinear dynamic time-history analyses of the prototype walls were conducted using the fiber element model (described in Kurama[1]) with a time step of 0.01 sec. Previous analyses[35] of similar walls show that the differences between results from analyses conducted using a time step of 0.001 and 0.01 sec. are not significant. Thus, the time step of 0.01 sec. is adequate to capture the dynamic characteristics of the walls.

The dynamic analyses were conducted with a viscous damping ratio of $\xi = 3$ percent in the first and third linear-elastic modes of vibration of the walls (using mass and stiffness proportional Rayleigh damping[22,23]). Similar to the loading condition used in design, the gravity loads acting on each wall were assumed to be equal to $1.00DL + 0.25LL$ as de-

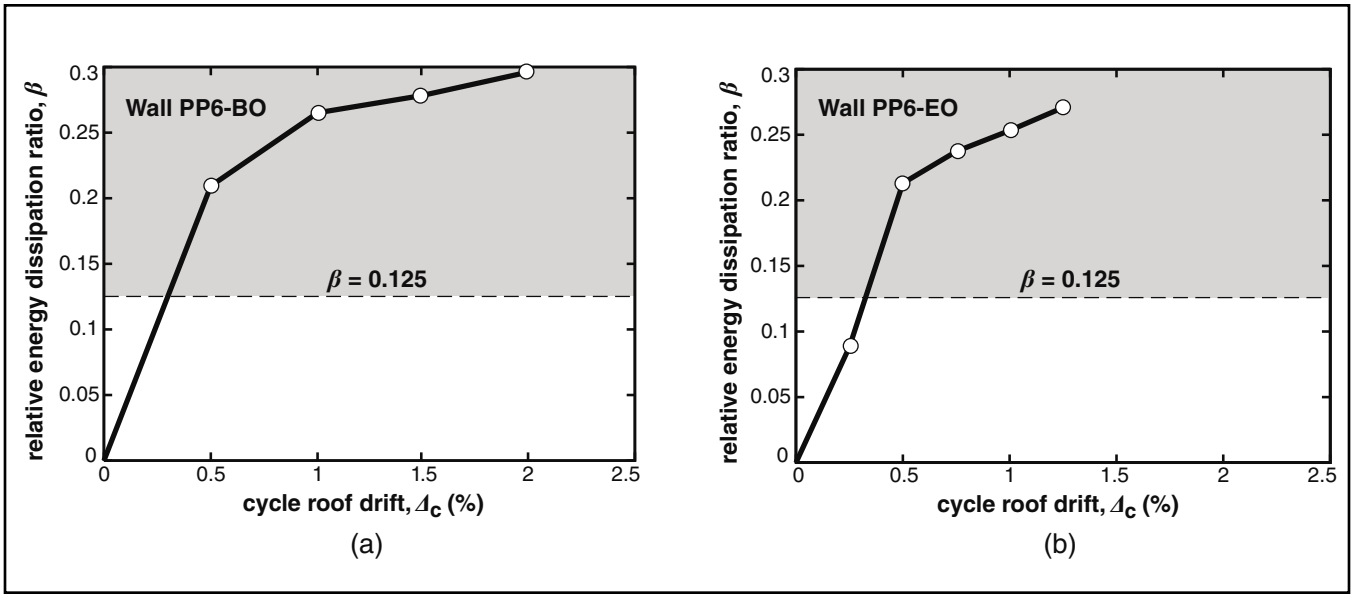

Fig. 7. Relative energy dissipation ratio, β: (a) Wall PP6-BO; (b) Wall PP6-EO.

scribed earlier. The total mass of each prototype building was assumed to be distributed equally among the walls used in that building. The masses assigned to the walls were lumped at the floor and roof fiber element nodes.

Ground Motion Records

A total of twenty ground motion records (Table 3) compiled and scaled by the SAC steel project[40] [SAC is a joint venture with the following partners: the Structural Engineers Association of California (SEAOC), the Applied Technology Council (ATC), and California Universities for Research in Earthquake Engineering (CUREE)] are used in this paper. This ground motion set corresponds to a probability of exceedence of 2 percent in 50 years (the same as the Maximum Considered Earthquake in IBC-2003[19]) and was compiled for a site in Los Angeles with a stiff soil profile, similar to the site soil condition used in the design of the prototype walls (i.e., Site Class D in IBC-2003[19]).

As described in Somerville et al.,[40] the acceleration time-histories of the twenty SAC ground motions in Table 3 were derived by scaling ten natural and ten generated records based on a target linear-elastic smooth acceleration response spectrum. The target response spectrum was determined from the probabilistic ground motion spectra published by the United States Geological Survey,[41,42] modified to represent Site Class D.

For each ground motion, two horizontal components, rotated 45 degrees away from the fault-normal and fault-parallel orientations, were used.[40] In order to preserve the variability in the characteristics of the individual ground motions, the shapes of the acceleration response spectra of the records were not modified in the SAC scaling procedure. Instead, for each ground motion, a single scale factor was found that minimized the weighted sum of the squared error between the average 5 percent damped SDOF linear-elastic acceleration response spectra of the two horizontal components and the target response spectrum in the period range of 0.3 to 4 secs.

More information on the generation and properties of the ground motion records, including SDOF linear-elastic acceleration response spectra, can be found in Somerville et al.[40] and Farrow and Kurama.[29,30]

Table 3 shows the factors that were used to scale the ground motion records, as well as the peak acceleration (*PGA*) and maximum incremental velocity (*MIV*) of the records. The *MIV* of a ground motion is equal to the maximum area under the acceleration time-history of the ground motion between two successive zero-acceleration crossings. The *PGA* values of the ground motions vary between 0.42*g* and 1.33*g* (where *g* is the gravitational acceleration) and the *MIV* values vary between 34.2 and 135 in./sec. (869 and 3429 mm/sec.), indicating a significant range in the seismic input intensity and characteristics.

Note that the validity of nonlinear dynamic time-history analysis results depends on the use of realistic ground motion records with phasing and response spectral characteristics that are appropriate for the magnitude, distance, site conditions, and wave propagation properties of the region. According to Somerville et al.,[40] the SAC ground motion records provide a sample of this variability through a set of time-histories that are realistic not only in their average properties, but also in their individual characteristics.

Nevertheless, it should be stated that the findings and conclusions presented in this paper are conditioned on the ability

Table 3. SAC ground motion records[40] used in the paper.

Ensemble	Site seismicity	Demand level	Site class	Record	Designation	Scale factor	*PGA* (*g*)	*MIV* (in./sec.)
SAC	Los Angeles, CA	Survival (2 percent in 50 years)	D	1995 Kobe	LA21	1.15	1.28	108
				1995 Kobe	LA22	1.15	0.92	95.1
				1989 Loma Prieta	LA23	0.82	0.42	34.2
				1989 Loma Prieta	LA24	0.82	0.47	82.9
				1994 Northridge	LA25	1.29	0.87	79.5
				1994 Northridge	LA26	1.29	0.94	106
				1994 Northridge	LA27	1.61	0.93	65.5
				1994 Northridge	LA28	1.61	1.33	88.9
				1974 Tabas	LA29	1.08	0.81	36.3
				1974 Tabas	LA30	1.08	0.99	50.3
				Generated, Elysian Park	LA31	1.43	1.30	81.8
				Generated, Elysian Park	LA32	1.43	1.19	102
				Generated, Elysian Park	LA33	0.97	0.78	73.9
				Generated, Elysian Park	LA34	0.97	0.68	63.5
				Generated, Elysian Park	LA35	1.10	0.99	135
				Generated, Elysian Park	LA36	1.10	1.10	130
				Generated, Palos Verdes	LA37	0.90	0.71	103
				Generated, Palos Verdes	LA38	0.90	0.78	119
				Generated, Palos Verdes	LA39	0.88	0.50	45.9
				Generated, Palos Verdes	LA40	0.88	0.63	110

Note: 1 in. = 25.4 mm.

of the selected ground motion set to suitably represent the site seismicity, seismic demand level, and soil condition used in the design of the prototype structures (i.e., Los Angeles, survival level, Site Class D).

Equivalent SDOF System for Design

It has been previously shown that,[24] for design purposes, the nonlinear lateral displacement response of a multi-degree-of-freedom (MDOF) structural wall system under earthquakes can be represented using an equivalent nonlinear SDOF system. This implies that the displacement response of the structure is controlled by the first mode, and that the shape of this mode remains essentially constant throughout the response history. Other researchers[43–45] have also shown that these assumptions lead to reasonable predictions of the maximum lateral displacement response of MDOF structures, provided that the response is dominated by the first mode.

As described previously, the estimation of the required wall design base moment strength in the proposed seismic design approach uses Eqs. (3) and (4) based on a nonlinear equivalent SDOF system, referred to as the BP system. The development of the BP system is described below using Wall PP6-BO.

First, the base shear versus roof drift (V-Δ) behavior of the wall in Fig. 6(b) is converted to an equivalent nonlinear SDOF force-displacement (R-s) relationship as shown in Fig. 8(a). As described in Kurama[24,25] and FEMA-274,[46] the SDOF force $R = V$ and the SDOF displacement $s = (h_w\Delta)/\Gamma$, where $\Gamma = L/M^*$ is referred to as the roof displacement participation factor and is calculated using the linear-elastic first mode shape of the wall. Then, the SDOF R-s relationship is idealized [Fig. 8(b)] by placing two simple hysteresis types in parallel [Fig. 8(c)]: (1) a bilinear-elastic (BE) hysteresis type; and (2) an elastic-perfectly-plastic (EP) hysteresis type. Note that the SDOF displacements, s, in Figs. 8(a) and 8(b) are shown as percentages of the wall height, h_w.

The combined system for the idealized SDOF relationship in Fig. 8(b) is referred to as the BP system, where the BE and EP components represent the contributions of the PT steel and the mild steel reinforcement to the wall base moment resistance, respectively. As described in Farrow and Kurama[30,47] and Kurama and Farrow,[48] the relationships between the lateral stiffnesses and strengths of the BE and EP components that make up a

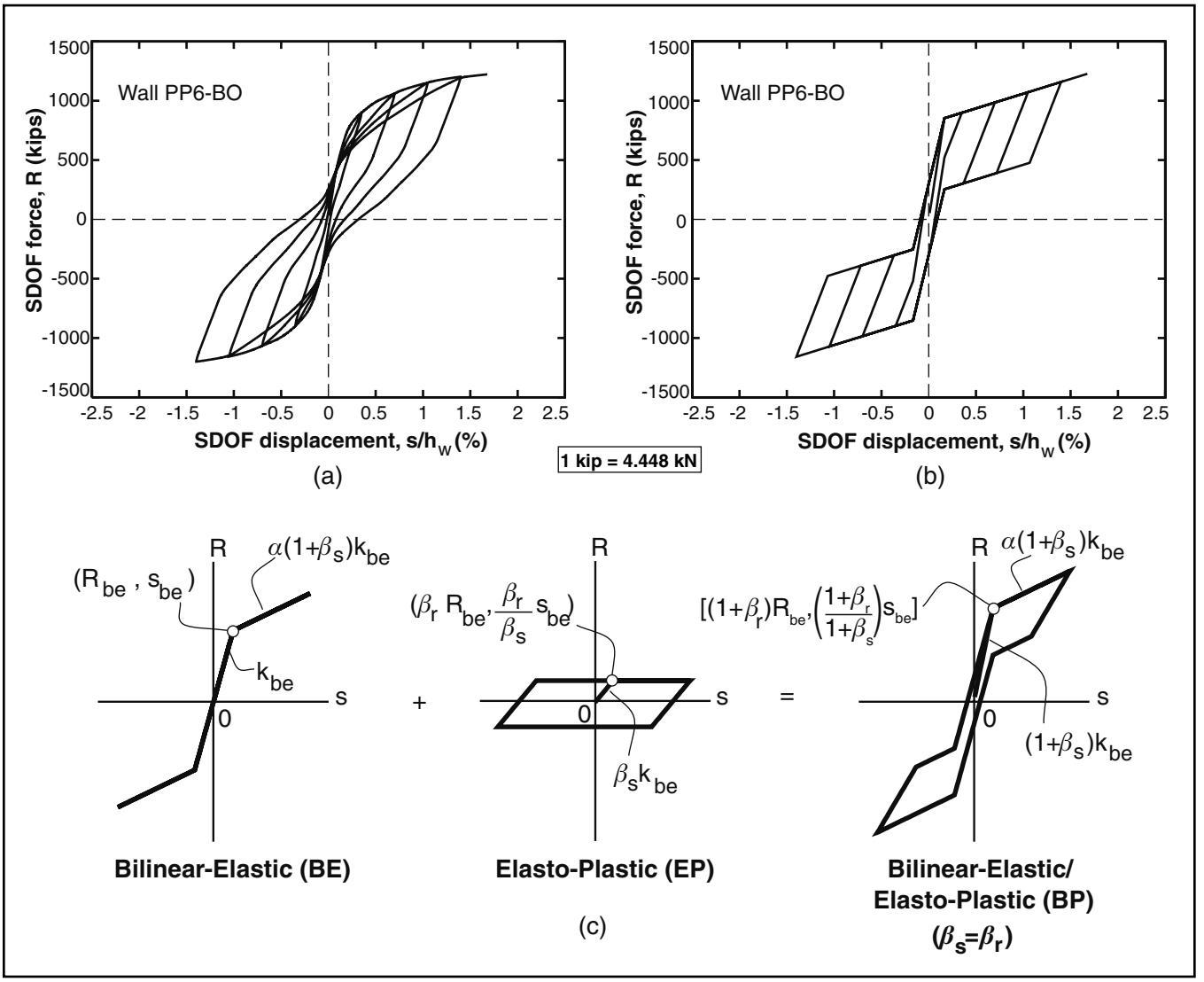

Fig. 8. Equivalent single-degree-of-freedom force-displacement (R-s) relationship: (a) smooth R-s relationship; (b) idealized BP system R-s relationship; (c) components of BP system.

BP system are: $k_{ep} = \beta_s k_{be}$ and $R_{ep} = \beta_r R_{be}$, where k_{be} and k_{ep} are the linear-elastic stiffnesses, R_{be} and R_{ep} are the yield strengths of the BE and EP components, respectively, and β_s and β_r are the BP system stiffness and strength ratios, respectively.

The energy dissipation of the BP system can be increased by increasing β_r. In this study, β_s is set equal to β_r. Such a system has only one yield point (since $\beta_s = \beta_r$) as illustrated in Fig. 8(c) and further discussed by Farrow and Kurama.[30]

Once the smooth SDOF *R-s* relationship of a wall [Fig. 8(a)] is obtained, the yield strengths R_{be} and R_{ep} and linear-elastic stiffnesses k_{be} and k_{ep} of the BE and EP components, as well as the post-yield stiffness ratio, α, for an idealized BP relationship [e.g., Fig. 8(b)] can be determined by equating: (1) the *R-s* relationship of the BP system with a bilinear ide-

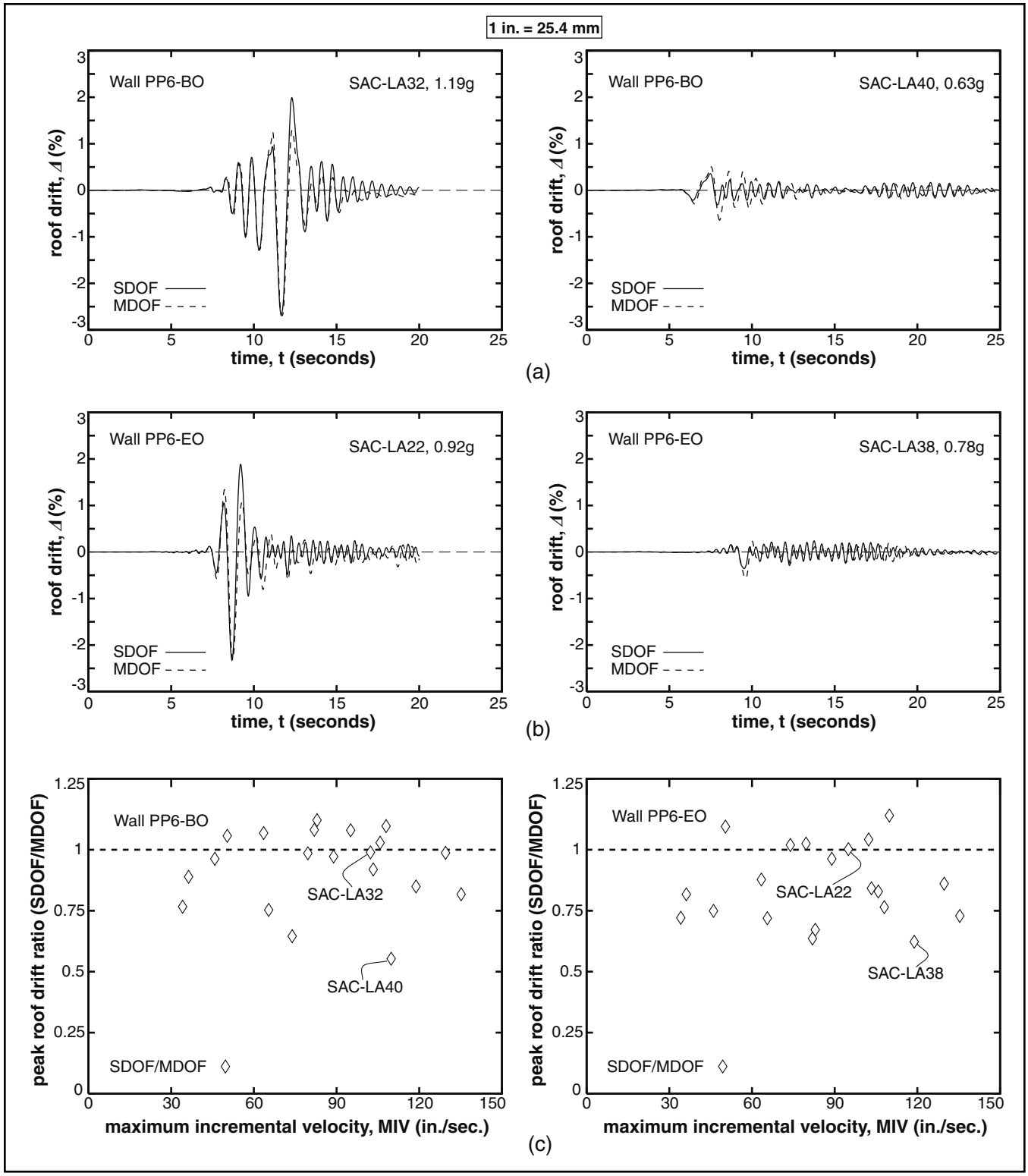

Fig. 9. Single-degree-of-freedom representation of the prototype walls: (a) roof drift time-history, Wall PP6-BO; (b) roof drift time-history, Wall PP6-EO; (c) peak roof drift ratio (SDOF/MDOF).

Table 4. Dynamic analysis results.

Wall	$\bar{\Delta}_p$ (percent)	Δ_d (percent)	Δ'_d (percent)	$\overline{\Delta_p/\Delta_d}$	$\overline{\Delta_p/\Delta'_d}$	$\bar{a}_p$ (g)
PP6-BO	1.65	2.37	1.79	0.69	0.92	1.54
PP6-EO	1.09	1.22	1.05	0.89	1.04	1.80

alization of the envelope of the smooth *R-s* relationship; and (2) the energy dissipated by the smooth *R-s* relationship with the energy dissipated by the BP idealization during a selected displacement cycle.

The mass of the equivalent SDOF system is assumed to be equal to the effective linear-elastic first mode mass of the structure divided by the number of walls as $m_{e1} = M_{e1}/n_w$. The linear-elastic period and damping ratio of the SDOF system are assumed to be equal to the linear-elastic first mode period, T_{e1}, and viscous damping ratio, ξ_{e1}, of the MDOF system, respectively.

Validation of SDOF BP System

In order to evaluate the ability of the equivalent nonlinear SDOF BP system described above to represent the dynamic displacement response of MDOF wall structures, Fig. 9(a) shows comparisons between the roof drift time-history of Wall PP6-BO using the MDOF model in Fig. 6(b) and the SDOF model in Fig. 8(b) under the SAC-LA32 and SAC-LA40 ground motion records (Table 3). The nonlinear dynamic time-history analyses of the MDOF system were conducted using the analytical wall model described in Kurama.[1] The wall roof drift values from the SDOF model were calculated as $\Delta = s\Gamma/h_w$, where $\Gamma = L/M^*$ is the roof displacement participation factor.

Similarly, Fig. 9(b) shows comparisons between the roof drift time-history of Wall PP6-EO in Fig. 6(c) and the roof drift time-history of the corresponding nonlinear SDOF BP system under the SAC-LA22 and SAC-LA38 ground motions.

Fig. 9(c) shows the ratios between the peak displacements of the SDOF BP systems and the corresponding MDOF systems for Walls PP6-BO and PP6-EO under the twenty SAC ground motions in Table 3. The results are plotted against the maximum incremental velocity (*MIV*) of the ground motions. The SAC-LA32 and SAC-LA40 ground motions in Fig. 9(a) result in the smallest and largest differences, respectively, between the peak displacements of the SDOF and MDOF systems for Wall PP6-BO (corresponding to SDOF/MDOF peak roof drift ratios of 0.99 and 0.56, respectively).

Similarly, the SAC-LA22 and SAC-LA38 ground motions in Fig. 9(b) result in the smallest and largest differences, respectively, between the peak displacements of the SDOF and MDOF systems for Wall PP6-EO (corresponding to SDOF/MDOF peak roof drift ratios of 1.01 and 0.62, respectively). It is observed that the largest percent differences between the displacements of the SDOF and MDOF models of the prototype walls occur under ground motion records for which the lateral displacements are relatively small (i.e., SAC-LA40 and SAC-LA38).

On average, the ratio between the peak displacements of the SDOF and MDOF models for Walls PP6-BO and PP6-EO is equal to 0.93 and 0.86, respectively. It is concluded that the nonlinear SDOF BP system is capable of representing both the roof drift time-history and the peak roof drift response of the prototype walls reasonably well.

As given in Eqs. (3) and (4), the proposed design approach uses the SDOF BP system to develop relationships between the lateral strength (quantified using the strength ratio R_1) and the displacement ductility demand, μ, of the walls. Nonlinear displacement ductility demands for SDOF BP systems have been studied extensively by Farrow and Kurama,[29,30] resulting in the mean *a* and *b* regression coefficients for the selected seismic design conditions (i.e., site seismicity, demand level, and site soil type) in Table 2.

The studies by Farrow and Kurama[29,30] show that the mean displacement ductility demands for BP systems are highly sensitive to the parameters of site seismicity, demand level, and site soil type; however, they are relatively insensitive to the BP system strength ratio, β_r. Based on these previous results, the *a* and *b* regression coefficients in Table 2 (which have been developed for BP systems with β_r = 1/3) can be reasonably used for the design of a wide range of partially post-tensioned precast concrete walls with mild steel moment ratios of up to $\beta_m = 1.0$.

MDOF Analysis Results

The behavior of Walls PP6-BO and PP6-EO under earthquake loading is evaluated with respect to the roof drift response (peak roof drift and roof drift time-history) and the peak roof acceleration.

Roof Drift Response—The ◊ markers in Fig. 10(a) show the peak roof drift, Δ_p, demands from the dynamic analyses of the walls under the twenty ground motion records in Table 3. The dashed horizontal lines represent the allowable target roof drift values of Δ_t = 2.4 and 1.2 percent used in the design of Walls PP6-BO and PP6-EO, respectively.

The mean peak roof drift demands from the dynamic analyses of Walls PP6-BO and PP6-EO are equal to $\bar{\Delta}_p$ = 1.65 and 1.09 percent, respectively (see Table 4). Since these mean demands are smaller than the corresponding target roof drift values, the design performance objectives for the walls are on average achieved.

The estimated peak roof drift demands of Walls PP6-BO and PP6-EO from Step 5 of the proposed design approach [i.e., Eq. (5)] are Δ_d = 2.37 and 1.22 percent, respectively (see Appendix B for Wall PP6-BO). As required by the design approach, these Δ_d values are close to the corresponding Δ_t values for the two walls. The mean values of the Δ_p/Δ_d ratios from the dynamic analyses of Walls PP6-BO and PP6-EO under the twenty ground motion records in Table 3 are equal to $\overline{\Delta_p/\Delta_d}$ = 0.69 and 0.89, respectively.

As examples of representative behavior, Fig. 10(b) shows the roof drift time-histories of Walls PP6-BO and PP6-EO under the SAC-LA31 and SAC-LA25 ground motions. The

peak roof drift demands of the walls under these records (Δ_p = 1.68 and 1.18 percent, respectively) are closest to the corresponding mean demands of $\overline{\Delta}_p$ = 1.65 and 1.09 percent, respectively.

The dashed horizontal lines in Fig. 10(b) represent the allowable target roof drift values of Δ_t = 2.4 and 1.2 percent used in the design of Walls PP6-BO and PP6-EO, respectively. The considerable difference between the mean and target displacement responses of Wall PP6-BO indicates that the proposed design approach has resulted in an overly conservative wall.

In order to investigate the possible source of this conservatism in design, the peak roof drift demands of Walls PP6-BO and PP6-EO under the twenty ground motions are compared with the mean peak roof drift demands estimated directly from the equivalent SDOF BP models of the two structures, without using the displacement ductility demand relationship given by Eqs. (3) and (4). These revised peak roof drift demand estimates are Δ'_d =1.79 and 1.05 percent, respectively. The resulting mean values of the Δ_p/Δ'_d ratios from the dynamic analyses of Walls PP6-BO and PP6-EO under the twenty ground motion records in Table 3 are equal to $\overline{\Delta_p/\Delta'_d}$ = 0.92 and 1.04, respectively.

These significantly improved demand estimates indicate that the BP system is capable of providing good representations, on average, of the peak displacement responses of Walls PP6-BO and PP6-EO; however, Eqs. (3) and (4) using the *a* and *b* regression coefficients in Table 2 result in conservative designs. Further research is needed to develop improved relationships between the lateral strength and the displacement ductility demand of partially post-tensioned precast concrete wall structures.

Note also that as observed in Fig. 10(a), there is a large scatter in the peak roof drift demands of the walls under the twenty SAC ground motion records. This scatter results in peak drift demands that are significantly larger than the target roof drift for some of the ground motion records, especially for Wall PP6-EO. The large scatter in the dynamic response of the walls may be due to a large variation in the intensity of the SAC ground motion records.

The peak roof drift demands in Fig. 10(a) appear to have a correlation with the maximum incremental velocity, *MIV*, of the ground motion records. The correlation is stronger for smaller values of *MIV* [*MIV* < 90 in./sec. (2286 mm/sec.)] than for larger values of *MIV*. These results indicate that it may be possible to obtain more uniform levels of seismic demand es-

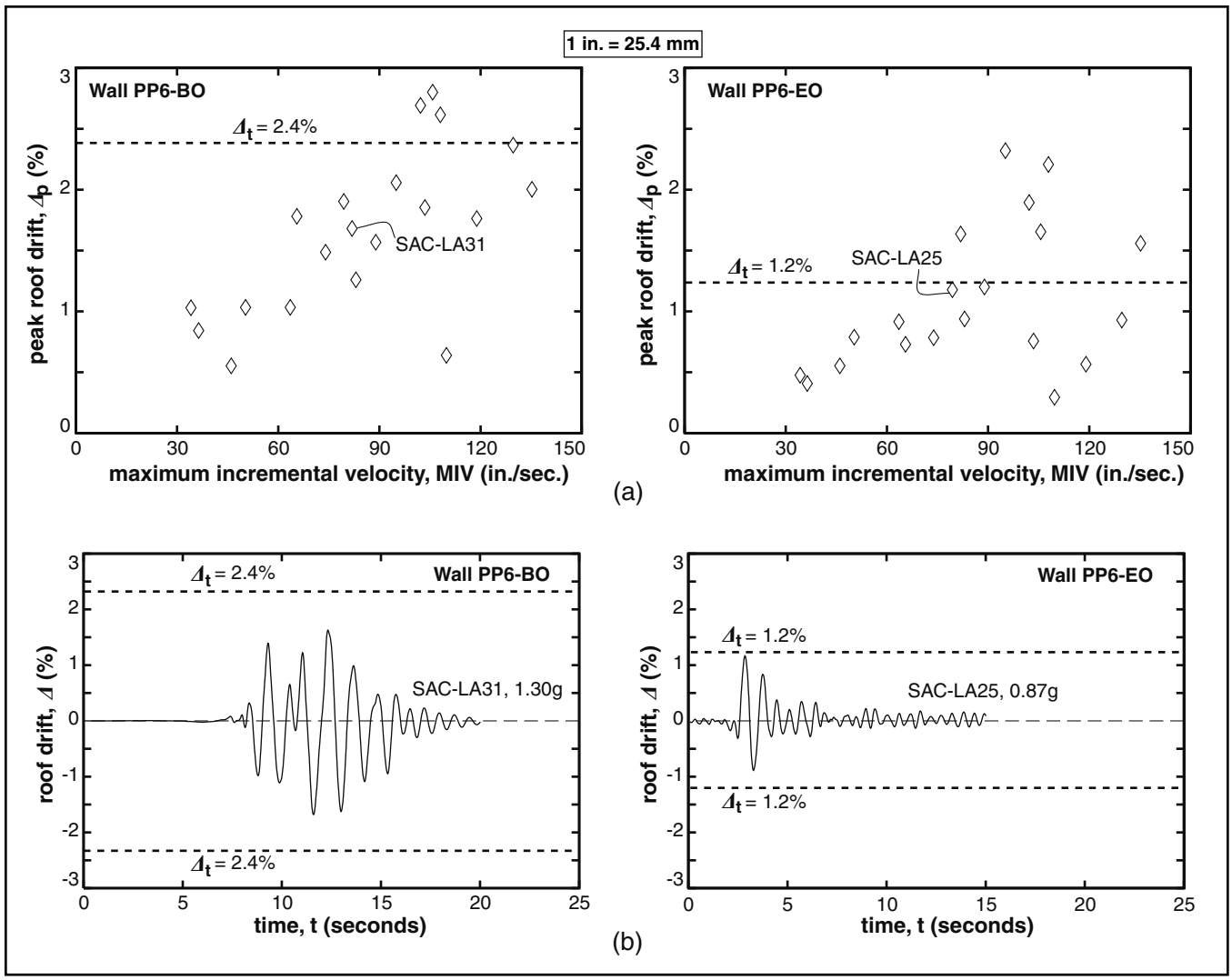

Fig. 10. Roof drift response of the prototype walls: (a) peak roof drift; (b) roof drift time-history.

timates (i.e., with reduced scatter) for the walls by scaling the ground motions to a constant value of *MIV* as investigated by Farrow and Kurama[30] and Kurama and Farrow.[48]

Note that other methods of ground motion scaling, such as to a constant spectral acceleration as recommended by Shome and Cornell[49] and Shome et al.,[50] may also reduce the scatter in the peak roof drift demands. The scaling of the ground motion records is not investigated further in this paper.

The roof drift time-history results in Figs. 9(a), 9(b), and 10(b) demonstrate the self-centering capability of the prototype walls as indicated by the oscillations about close to the zero-drift position, with little residual (i.e., permanent) displacements at the end of the ground motions. The results also show that the displacement responses of the walls decay (i.e., decrease) at a reasonable rate.

As shown by Kurama,[1] the decay in the displacement response of the walls occurs primarily as a result of the energy dissipation provided by the yielding of the bonded mild steel reinforcement crossing the horizontal joints. This behavior is one of the potential advantages of using partially post-tensioned precast concrete walls as compared with fully post-tensioned walls (with no mild steel reinforcement), which may experience a larger number of large drift peaks during a ground motion due to a considerably smaller amount of decay in the dynamic response.

Roof Acceleration Response—Fig. 11 shows the peak absolute roof acceleration, a_p (where the absolute acceleration is calculated as the relative acceleration of the roof with respect to the ground plus the ground acceleration), from the dynamic analyses of the prototype walls. The mean peak acceleration of Walls PP6-BO and PP6-EO is equal to $\bar{a}_p$ = 1.54*g* and 1.80*g*, respectively. While the scatter in the peak acceleration of the walls under the twenty SAC ground motion records is large, no significant correlation is observed with *MIV*.

Note that, unlike the lateral displacement response of the walls, the acceleration response may be significantly affected by higher modes of vibration.[51] Thus, the SDOF BP system described previously should not be used to estimate the peak wall accelerations.

CONCLUSIONS

This paper proposes a seismic design approach for precast concrete structural walls that use a combination of mild steel and high strength post-tensioning (PT) steel reinforcement for lateral resistance. These walls are referred to as partially post-tensioned walls in this paper. The proposed seismic design approach is a performance based approach that aims to limit the wall lateral displacements to an allowable target displacement. The design approach is critically evaluated based on nonlinear static and nonlinear dynamic time-history analyses of two prototype walls. The following conclusions can be drawn from the investigation:

1. Nonlinear static reversed cyclic lateral load analyses of the prototype walls indicate stable behavior with considerable inelastic energy dissipation and self-centering capability. It is shown that the energy dissipation requirement of the draft ACI ITG T5.1 document[12,13] can be satisfied by using bonded mild steel reinforcement crossing the horizontal joint between the wall and the foundation. Previous investigations[1] have concluded that fully post-tensioned walls with no mild steel reinforcement crossing the horizontal joints do not satisfy this requirement.

2. As compared with monolithic cast-in-place reinforced concrete walls, the amount of mild steel reinforcement that would be needed in a partially post-tensioned precast wall is smaller, because a portion of the lateral strength of the wall is provided by the post-tensioning steel.

3. The mild steel moment ratio, β_m, introduced in the paper is a design parameter to specify the relative contribution of the mild steel reinforcement to the total base moment resis-

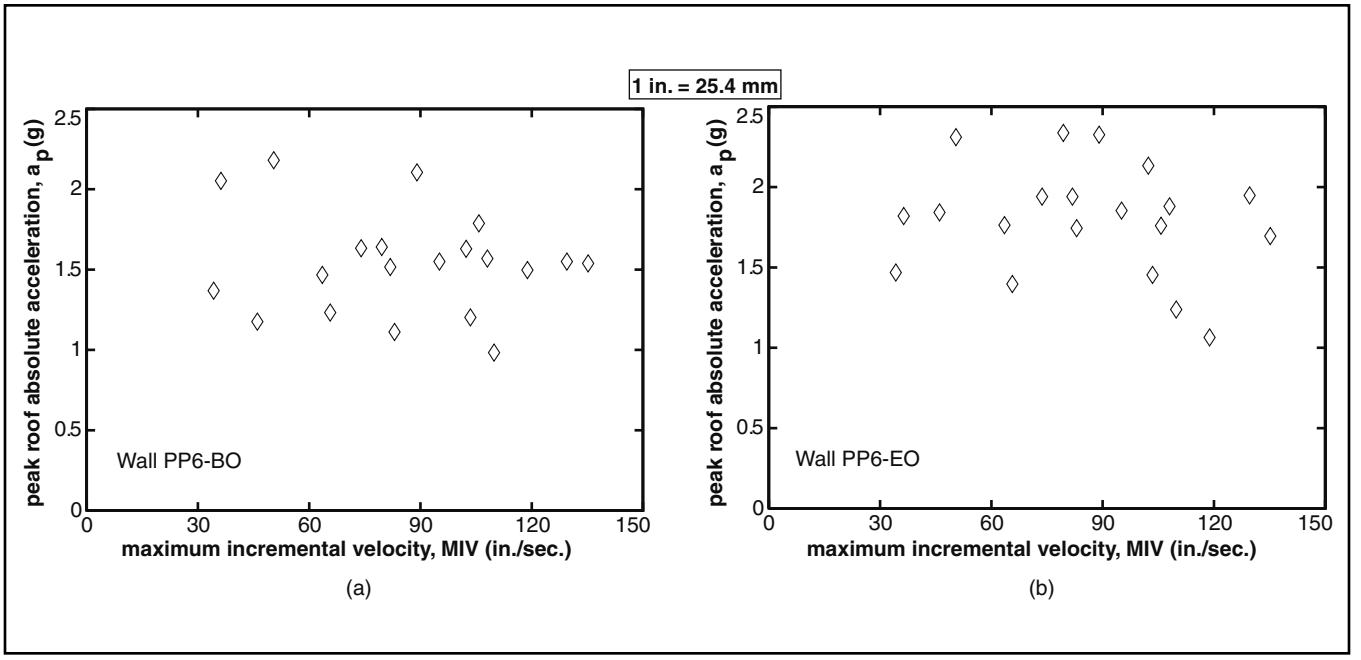

Fig. 11. Peak roof absolute acceleration of the prototype walls: (a) Wall PP6-BO; (b) Wall PP6-EO.

tance of a wall. Systems with larger β_m values correspond to walls with larger amounts of mild steel reinforcement. If the mild steel contribution is too small (i.e., the β_m value is too small), then the inelastic energy dissipation of the structure may not satisfy the ACI ITG T5.1[12,13] requirement. A value of $0.75 \le \beta_m \le 1$ is recommended for design.

4. The proposed design approach can be used to achieve selected seismic performance objectives for the walls, including basic objectives (e.g., to prevent crushing of the confined concrete at the wall base) and enhanced objectives (e.g., to prevent yielding of the PT steel in addition to crushing of the confined concrete). Design guidelines are provided in the paper to determine the areas of the PT steel and mild steel reinforcement in a wall, as well as the amount of concrete confinement needed. Additional recommendations are provided on the detailing of the mild steel reinforcement and on shear design.

5. The proposed seismic design approach uses peak displacement ductility demand regression relationships based on an equivalent nonlinear single-degree-of-freedom (SDOF) system, referred to as the BP system. Nonlinear dynamic time-history analyses indicate that the equivalent SDOF BP system provides an effective tool to estimate the lateral displacement response of multi-degree-of-freedom partially post-tensioned precast concrete walls under earthquake loading.

6. Nonlinear dynamic time-history analyses of the prototype walls under twenty selected ground motion records show that the mean peak lateral displacement demand for each wall is less than the corresponding allowable target displacement used in design. Thus, the seismic performance objectives used in the design of the walls are on average achieved.

7. While the design performance objectives are on average achieved, the dynamic analysis results also indicate that the proposed displacement ductility demand regression relationships result in somewhat overly conservative designs for the prototype structures. Further research is needed to develop improved relationships between the lateral strength and the displacement ductility demand of partially post-tensioned precast concrete walls.

8. There is significant scatter in the peak lateral displacement demands of the prototype walls under the twenty selected ground motion records, possibly due to a large variation in the intensity of the ground motions. This scatter results in peak displacement demands that are significantly larger than the design allowable target displacement under some of the ground motion records.

9. The dynamic analysis results indicate that it may be possible to obtain more uniform levels of seismic displacement demand estimates for the walls by scaling the ground motion records to a constant maximum incremental velocity (*MIV*).

10. The dynamic roof displacement time-history results demonstrate the large self-centering capability of the prototype walls as indicated by the oscillations about close to the zero-displacement position, with little residual (i.e., permanent) displacement at the end of a ground motion.

11. The dynamic analysis results also show that the lateral displacement responses of the walls decay (i.e., decrease) at a reasonable rate. This occurs due to, primarily, the energy dissipation provided by the yielding of the mild steel reinforcement and is one of the potential advantages of partially post-tensioned precast concrete walls as compared with fully post-tensioned walls with no mild steel reinforcement.

12. The peak absolute roof accelerations of the prototype walls do not appear to have a strong correlation with the ground motion intensity.

ACKNOWLEDGMENTS

This investigation was funded by the National Science Foundation (NSF) under Grant No. CMS 98-74872 as a part of the CAREER Program. The support of the NSF program directors, Dr. Shih Chi Liu and Dr. Steven L. McCabe, is gratefully acknowledged. The author also expresses his gratitude to the PCI JOURNAL reviewers for their thoughtful and constructive comments.

The opinions, findings, and conclusions expressed in the paper are those of the author and do not necessarily reflect the views of the NSF or the program directors acknowledged above.

REFERENCES

1. Kurama, Y., "Hybrid Post-Tensioned Precast Concrete Walls for Use in Seismic Regions," PCI JOURNAL, V. 47, No. 5, September-October 2002, pp. 37-59.
2. Rahman, A., and Restrepo, J., "Earthquake Resistant Precast Concrete Buildings: Seismic Performance of Cantilever Walls Prestressed Using Unbonded Tendons," Report No. 2000-5, Department of Civil Engineering, University of Canterbury, Christchurch, New Zealand, 2000.
3. Holden, T., Restrepo, J., and Mander, J., "A Comparison of the Seismic Performance of Precast Wall Construction: Emulation and Hybrid Approaches," Rep. No. 2001-4, Department of Civil Engineering, University of Canterbury, Christchurch, New Zealand, 2001.
4. Holden, T., Restrepo, J., and Mander, J., "Seismic Performance of Precast Reinforced and Prestressed Concrete Walls," *Journal of Structural Engineering*, ASCE, V. 129, No. 3, March 2003, pp. 286-296.
5. Restrepo, J., "Self-Centering Precast Post-Tensioned Cantilever Walls—Theory and Experimental Work," ASCE Structures Congress, Seattle, WA, May 29-31, 2003.
6. Cheok, G., and Stone, W., "Performance of 1/3-Scale Model Precast Concrete Beam-Column Connections Subjected to Cyclic Inelastic Loads—Report No. 4," NISTIR 5436, National Institute of Standards and Technology (NIST), Gaithersburg, MD, June 1994.
7. Stone, W., Cheok, G., and Stanton, J., "Performance of Hybrid Moment-Resisting Precast Beam-Column Concrete Connections Subjected to Cyclic Loading," *ACI Structural Journal*, V. 91, No. 2, March-April 1995, pp. 229-249.
8. Stanton, J., Stone, W., and Cheok, G., "A Hybrid Reinforced Precast Frame for Seismic Regions," PCI JOURNAL, V. 42, No. 2, March-April 1997, pp. 20-32.
9. Cheok, G., Stone, W., Kunnath, S., "Seismic Response of Precast Concrete Frames with Hybrid Connections," *ACI Structural Journal*, V. 95, No. 5, September-October 1998, pp. 527-539.
10. Nakaki, S. D., Stanton, J. F., and Sritharan, S., "An Overview of the PRESSS Five-Story Precast Test Building," PCI JOURNAL, V. 44, No. 2, March-April 1999, pp. 26-39.
11. Priestley, M., Sritharan, S., Conley, J., and Pampanin, S., "Preliminary Results and Conclusions from the PRESSS Five-Story Precast Concrete Test Building," PCI JOURNAL, V. 44,

No. 6, November-December 1999, pp. 42-67.
12. ACI Innovation Task Group 5 and Collaborators, "Acceptance Criteria for Special Precast Structural Walls Based on Validation Testing and Commentary," Draft, ITG T5.1, American Concrete Institute, Farmington Hills, MI, 2004.
13. Hawkins, N., and Ghosh, S., "Acceptance Criteria for Special Precast Concrete Structural Walls Based on Validation Testing," PCI JOURNAL, V. 49, No. 5, September-October 2004, pp. 78-92.
14. Cheok, G., Stone, W., and Nakaki, S., "Simplified Design Procedure for Hybrid Precast Concrete Connections," NISTIR 5765, National Institute of Standards and Technology, Gaithersburg, MD, 1996, 81 pp.
15. ACI Innovation Task Group 1 and Collaborators, "Special Hybrid Moment Frames Composed of Discretely Jointed Precast and Post-Tensioned Concrete Members (ACI T1.2-XX) and Commentary (T1.2R-XX)," *ACI Structural Journal*, V. 98, No. 5, September-October 2001, pp. 771-784.
16. ACI Innovation Task Group 1 and Collaborators, "Special Hybrid Moment Frames Composed of Discretely Jointed Precast and Post-Tensioned Concrete Members," ACI Proposed Standard T1.2-03 and Commentary ACI T1.2R-03, American Concrete Institute, Farmington Hills, MI, 2003.
17. Stanton, J., and Nakaki, S., "Design Guidelines for Precast Concrete Seismic Structural Systems," PRESSS Report No. 01/03-09, UW Report No. SM 02-02, Department of Civil Engineering, University of Washington, Seattle, WA, February 2002.
18. Englekirk, R., "Design-Construction of The Paramount—A 39-Story Precast Prestressed Concrete Apartment Building," PCI JOURNAL, V. 47, No. 4, July-August 2002, pp. 56-71.
19. ICC, *International Building Code 2003*, International Code Council, Falls Church, VA, 2003.
20. Paulay, P., and Priestley, M., *Seismic Design of Reinforced Concrete and Masonry Buildings*, John Wiley & Sons, Inc., New York, NY, 1992, 744 pp.
21. Mander, J., Priestley, M., and Park, R., "Theoretical Stress-Strain Model for Confined Concrete," *Journal of Structural Engineering*, ASCE, V. 114, No. 8, August 1988, pp. 1804-1826.
22. Chopra, A., *Dynamics of Structures: Theory and Applications to Earthquake Engineering,* Second Edition, Prentice Hall, Inc., New York, NY, 2001, 844 pp.
23. Clough, R., and Penzien, J., *Dynamics of Structures*, Second Edition, McGraw-Hill, Inc., New York, NY, 1993, 738 pp.
24. Kurama, Y., "Simplified Seismic Design Approach for Friction-Damped Unbonded Post-Tensioned Precast Concrete Walls," *ACI Structural Journal*, V. 98, No. 5, September-October 2001, pp. 705-716.
25. Kurama, Y., "Seismic Design of Unbonded Post-Tensioned Precast Walls with Supplemental Viscous Damping," *ACI Structural Journal*, V. 97, No. 4, July-August 2000, pp. 648-658.
26. AIJ, "AIJ Recommendations for the Design of Base Isolated Buildings," Architectural Institute of Japan, Tokyo, Japan, 1993.
27. FEMA, "Prestandard and Commentary for the Seismic Rehabilitation of Buildings (FEMA-356)," Federal Emergency Management Agency, Washington, DC, 2000.
28. Nassar, A., and Krawinkler, H., "Seismic Demands for SDOF and MDOF Systems," John A. Blume Earthquake Engineering Center, Report No. 95, Department of Civil Engineering, Stanford University, Palo Alto, CA, June 1991.
29. Farrow, K., and Kurama, Y., "SDOF Demand Index Relationships for Performance-Based Seismic Design," *Earthquake Spectra*, Earthquake Engineering Research Institute, Berkeley, CA, V. 19, No. 4, November 2003, pp. 799-838.
30. Farrow, K., and Kurama, Y., "Capacity-Demand Index Relationships for Performance-Based Seismic Design," Structural Engineering Research Report #NDSE-01-02, Department of Civil Engineering and Geological Sciences, University of Notre Dame, Notre Dame, IN, November 2001, 259 pp. (available for download at http://www.nd.edu/~concrete)
31. ACI Committee 318, "Building Code Requirements for Structural Concrete (ACI 318) and Commentary (ACI 318R)," American Concrete Institute, Farmington Hills, MI, 2002.
32. Ghosh, S., and Markevicius, V., "Design of Earthquake Resistant Shearwalls to Prevent Shear Failure," Fourth U.S. National Conference on Earthquake Engineering, Earthquake Engineering Research Institute, Berkeley, CA, V. 2, 1990, pp. 905-913.
33. Aoyama, H., "Earthquake Resistant Design of Reinforced Concrete Frame Buildings with Flexural Walls," in *Earthquake Resistance of Reinforced Concrete Structures, A Volume Honoring Hiroyuki Aoyama,* Editor: T. Okada, Department of Architecture, Faculty of Engineering, University of Tokyo, Tokyo, Japan, 1993, pp. 78-100.
34. Eberhard, M., and Sozen, M., "Behavior-Based Method to Determine Design Shear in Earthquake-Resistant Walls," *Journal of Structural Engineering*, ASCE, V. 119, No. 2, 1993, pp. 619-640.
35. Kabeyasawa, T., "Ultimate-State Design of Wall-Frame Structures," in *Earthquake Resistance of Reinforced Concrete Structures, A Volume Honoring Hiroyuki Aoyama,* Editor: T. Okada, Department of Architecture, Faculty of Engineering, University of Tokyo, Tokyo, Japan, 1993, pp. 431-440.
36. Kurama, Y., Sause, R., Pessiki, S., Lu, L.W., and El-Sheikh, M., "Seismic Design and Response Evaluation of Unbonded Post-Tensioned Precast Concrete Walls," Research Report No. EQ-97-01, Department of Civil and Environmental Engineering, Lehigh University, Bethlehem, PA, 1997, 184 pp.
37. Kurama, Y., Pessiki, S., Sause, R., and Lu, L.W., "Seismic Behavior and Design of Unbonded Post-Tensioned Precast Concrete Walls," PCI JOURNAL, V. 44, No. 3, May-June 1999, pp. 72-89.
38. Kurama, Y., Sause, R., Pessiki, S., and Lu, L.W., "Seismic Response Evaluation of Unbonded Post-Tensioned Precast Walls," *ACI Structural Journal*, V. 99, No. 5, September-October 2002, pp. 641-651.
39. Allen, M., and Kurama, Y., "Design of Rectangular Openings in Precast Walls Under Combined Vertical and Lateral Loads," PCI JOURNAL, V. 47, No. 2, March-April 2002, pp. 58-83.
40. Somerville, P., Smith, N., Punyamurthula, S., and Sun, J., "Development of Ground Motion Time Histories for Phase 2 of the FEMA/SAC Steel Project," SAC/BD-97/04, SAC, Sacramento, CA, 1997.
41. Frankel, A., Mueller, C., Barnhard, T., Perkins, D., Leyendecker, E., Dickman, N., Hanson, S., and Hopper, M., "National Seismic Hazard Maps, June 1996: Documentation," U.S. Geological Survey, Open-File Report 96-532, 1996.
42. Building Seismic Safety Council (BSSC), "NEHRP Recommended Provisions for Seismic Regulations for New Buildings and Other Structures," FEMA 302, Federal Emergency Management Agency, Washington, DC, 1998.
43. Saiidi, M., and Sozen, M., "Simple Nonlinear Seismic Analysis of R/C Structures," *Journal of Structural Engineering*, ASCE, V. 107, No. ST5, 1981, pp. 937-951.
44. Fajfar, P., and Fischinger, M., "N2-A Method for Non-Linear Seismic Analysis of Regular Structures," *Ninth World Conference on Earthquake Engineering*, Tokyo, Japan, 1988.
45. Qi, X., and Moehle, J., "Displacement Design Approach for Reinforced Concrete Structures Subjected to Earthquakes,"

Report No. EERC 91/02, Earthquake Engineering Research Center, University of California, Berkeley, CA, 1991.
46. FEMA, "NEHRP Commentary on the Guidelines for the Seismic Rehabilitation of Buildings," FEMA 274, Federal Emergency Management Agency, Washington, DC, 1997.
47. Farrow, K., and Kurama, Y., "SDOF Displacement Ductility Demands Based on Smooth Ground Motion Response Spectra," *Engineering Structures*, Elsevier, V. 26, No. 12, October 2004, pp. 1713-1733.
48. Kurama, Y., and Farrow, K., "Ground Motion Scaling Methods for Different Site Conditions and Structure Characteristics," *Earthquake Engineering and Structural Dynamics*, V. 32, No. 15, December 2003, pp. 2425-2450.
49. Shome, N., and Cornell, C., "Normalization and Scaling Accelerograms for Nonlinear Structural Analysis," Sixth U.S. National Conference on Earthquake Engineering, Seattle, WA, May-June 1998 (CD-ROM).
50. Shome, N., Cornell, C., Bazzurro, P., and Carballo, J., "Earthquakes, Records, and Nonlinear Responses," *Earthquake Spectra*, Earthquake Engineering Research Institute, V. 14, 1998, pp. 469-500.
51. Rodriguez, M., Restrepo, J., and Carr, A., "Earthquake-Induced Floor Horizontal Accelerations in Buildings," *Earthquake Engineering and Structural Dynamics*, V. 31, No. 3, March 2002, pp. 693-718.

APPENDIX A – NOTATION

a = displacement ductility demand regression coefficient
a_c = length of concrete rectangular (i.e., uniform) compressive stress block at wall base
a_p = area of a post-tensioning tendon
a_p = peak absolute roof acceleration
$\overline{a}_p$ = mean peak absolute roof acceleration
A_p = total area of post-tensioning steel reinforcement in wall
A_s = total area of mild steel reinforcement on tension side of wall
A'_s = total area of mild steel reinforcement on compression side of wall
b = displacement ductility demand regression coefficient
c = displacement ductility demand regression coefficient
c_c = neutral axis depth at wall base
c_{cu} = neutral axis depth at wall base corresponding to crushing of confined concrete
c_{py} = neutral axis depth at wall base corresponding to "yielding" of post-tensioning steel
C = total compressive stress resultant at wall base
d_{py} = distance from compression end of wall to post-tensioning tendon with largest strain
d_{sc} = distance from compression end of wall to centroid of A_s
d'_{sc} = distance from compression end of wall to centroid of A'_s
d_{si} = distance from compression end of wall to innermost tension-side mild steel bar
d'_{si} = distance from compression end of wall to innermost compression-side mild steel bar
d_{so} = distance from compression end of wall to outermost tension-side mild steel bar
d_{sp} = wire diameter of concrete confinement spiral
D_h = area enclosed by a wall V-Δ hysteresis loop
D_{sp} = center-to-center diameter of concrete confinement spiral
DL = unfactored design dead load
E_c = Young's modulus of concrete
E_p = Young's modulus of post-tensioning steel
E_{py} = "post-yield" stiffness of post-tensioning steel
E_s = Young's modulus of mild steel reinforcement
EQ = design earthquake load
f'_c = compressive strength of unconfined concrete
f'_{cc} = compressive strength of confined concrete
f_{cu} = confined concrete stress corresponding to ε_{cu}
f_p = stress in post-tensioning steel
f_{pi} = initial stress in post-tensioning steel after losses
f_{pu} = ultimate (peak) strength of post-tensioning steel
f_{py} = "yield" (i.e., linear limit) strength of post-tensioning steel
f_s = mild steel stress at centroid of A_s at wall base
f'_s = mild steel stress at centroid of A'_s at wall base
f_{spy} = yield strength of spiral steel
f_{su} = ultimate (peak) strength of mild steel reinforcement
f_{sy} = yield strength of mild steel reinforcement
f_ξ = damping adjustment coefficient
F_a = site coefficient for short periods from IBC-2003[19]
F_v = site coefficient for 1-sec. period from IBC-2003[19]
g = acceleration due to gravity
G_{dl} = total axial force at wall base due to unfactored design dead loads
G_{ll} = total axial force at wall base due to unfactored unreduced design live loads
h_c = height of wall where concrete confinement is needed at base
h_w = height of wall
h_{wp} = "plastic hinge" height at wall base
H_v = resultant height of linear-elastic first (i.e., fundamental) mode inertia forces
k_{be} = linear-elastic stiffness of BE component of single-degree-of-freedom BP system
k_{ep} = linear-elastic stiffness of EP component of single-degree-of-freedom BP system
K_i = structure linear-elastic lateral stiffness
K_{wi} = wall linear-elastic lateral stiffness
l_c = length of wall at each end where concrete confinement is needed at base
l_{pu} = unbonded length of post-tensioning steel

l_w = length of wall
L = earthquake excitation factor
LL = unfactored unreduced design live load
m_{e1} = effective linear-elastic first (i.e., fundamental) mode mass of wall
$[M]$ = diagonal mass matrix for structure
M^* = generalized linear-elastic first (i.e., fundamental) mode mass of structure
M_{e1} = effective linear-elastic first (i.e., fundamental) mode mass of structure
M_{wd} = wall design base moment demand
M_{wn} = contribution of wall applied (external) axial load to wall base moment strength
M_{wp} = contribution of post-tensioning steel reinforcement to wall base moment strength
M_{ws} = contribution of mild steel reinforcement to wall base moment strength
M_{wy} = wall nominal "yield" moment strength
MIV = ground motion maximum incremental velocity
n_p = number of post-tensioning tendons in wall cross section
n_w = number of walls in structure
N_{wd} = wall factored design axial force at base
PGA = ground motion peak acceleration
R = force in equivalent single-degree-of-freedom system
R_{be} = yield strength of BE component of single-degree-of-freedom BP system
R_{ep} = yield strength of EP component of single-degree-of-freedom BP system
R_1 = strength ratio
s = displacement of equivalent single-degree-of-freedom system
s_{be} = yield displacement of single-degree-of-freedom BP system
s_{sp} = pitch of confinement spiral
S = site adjusted linear-elastic design spectral response acceleration
S_{MS} = Maximum Considered Earthquake spectral response acceleration for short periods[19]
S_{M1} = Maximum Considered Earthquake spectral response acceleration for 1-sec. period[19]
S_s = mapped spectral response acceleration for short periods
S_1 = mapped spectral response acceleration for 1-sec. period
t = time
t_w = thickness of wall
T_{e1} = linear-elastic first (i.e., fundamental) mode period of wall/structure
u_{py} = elongation of post-tensioning steel from f_{pi} to f_{py}
V = base shear force
V_{sd} = structure design base shear demand
V_{ss} = wall nominal shear slip strength
V_{wd} = wall design base shear demand
$V_{w,max}$ = peak wall base shear demand
W_s = total structure seismic weight
α = post-yield stiffness ratio of single-degree-of-freedom BP system
β = relative energy dissipation ratio[12,13]
β_m = mild steel moment ratio
β_r = strength ratio of single-degree-of-freedom BP system
β_s = stiffness ratio of single-degree-of-freedom BP system
β_1 = concrete rectangular stress block parameter
Γ = roof displacement participation factor ($\Gamma = L/M^*$)
Δ = roof drift (roof lateral displacement divided by wall height)
Δ_c = maximum/minimum roof drift for a hysteresis cycle
Δ_d = estimated design roof drift demand (from Step 5 of proposed design approach)
Δ'_d = mean roof drift demand from dynamic analyses of equivalent single-degree-of-freedom BP system
Δ_p = peak roof drift demand from multi-degree-of-freedom dynamic analysis
$\overline{\Delta}_p$ = mean peak roof drift demand from multi-degree-of-freedom dynamic analyses
Δ_{py} = roof drift corresponding to "yielding" of post-tensioning steel
$\overline{\Delta_p/\Delta_d}$ = mean value of Δ_p/Δ_d ratios from dynamic analyses
$\overline{\Delta_p/\Delta'_d}$ = mean value of Δ_p/Δ'_d ratios from dynamic analyses
Δ_t = allowable target roof drift used in design
ε_{cu} = ultimate (crushing) strain of confined concrete
ε_{c0} = confined concrete strain corresponding to f'_{cc}
ε_{si} = strain in innermost tension-side mild steel bar at wall base
ε'_{si} = strain in innermost compression-side mild steel bar at wall base
ε_{sm} = maximum strain in outermost tension-side mild steel bar at wall base
ε_{spm} = strain in spiral steel at peak strength
ε_u = ultimate (crushing) strain of unconfined concrete
ε_0 = unconfined concrete strain corresponding to f'_c
μ = roof displacement ductility demand
μ_s = design coefficient of friction for shear slip
μ_t = roof displacement ductility demand corresponding to Δ_t
ξ = viscous damping ratio
ξ_{e1} = linear-elastic first (i.e., fundamental) mode viscous damping ratio
ξ_0 = viscous damping ratio corresponding to S/R_1 value used in design
ϱ_p = post-tensioning steel ratio (total post-tensioning steel area/wall cross-section area)
ϱ_s = mild steel reinforcement ratio (total mild steel area/wall cross-section area)
ϱ_{sp} = concrete confinement spiral reinforcement ratio
ϕ_{cu} = curvature at wall base at crushing of confined concrete
$\{\phi_{e1}\}$ = linear-elastic first (i.e., fundamental) mode shape of wall/structure

APPENDIX B – DESIGN EXAMPLE

The following example demonstrates the design of Wall PP6-BO (see Fig. B1) using the proposed seismic design approach. Note that while this example includes the main features of the seismic design of a partially post-tensioned precast concrete wall, it is not a complete design example.

The following assumptions and simplifications are made for the design:

1. The floor diaphragms are assumed to be rigid.
2. Seismic loads out of the plane of the walls are ignored (only loads in the direction of the walls are considered).
3. Torsional effects on the building (including accidental torsion effects) are ignored.
4. Vertical ground acceleration effects are ignored.
5. The walls are designed for a single hypothetical load combination of $1.0DL + 0.25LL + 1.0EQ$, where DL is the design dead load, LL is the design live load, and EQ is the earthquake load. Note that this load combination is different than the combinations specified in IBC-2003[19] and should not be used in practice.
6. No capacity reduction factors are used in the design of the walls.
7. The distribution of the equivalent lateral forces over the height of the walls is assumed to be equal to the linear-elastic first mode distribution of inertia forces.
8. The wall foundations are assumed to be rigid.

General Design Information

Building type: Office.
Number of stories = 6.
Story heights = 16 ft (4.88 m) for first story and 13 ft (3.96 m) for other stories.
Building plan: See Fig. B1.
Building location: Los Angeles, California.
Site class: D (stiff).[19]
Seismic demand level: Survival (2 percent in 50 years).
Mapped spectral response accelerations from IBC-2003:[19]
– For short periods, $S_s = 2.05g$.
– For 1-sec. period, $S_1 = 0.81g$.
Design objective: Prevent crushing of confined concrete.
Allowable target roof drift, $\Delta_t = 2.4$ percent.
Gravitational acceleration, $g = 386.1$ in./sec.^{2} (9.81 m/sec.^{2}).

Lateral Load System in the N-S direction

System type: Partially post-tensioned precast concrete walls.
Number of walls, $n_w = 10$.
Wall length, $l_w = 20$ ft (6.10 m).
Wall height, $h_w = 16 + (5)(13) = 81$ ft (24.7 m).
Wall aspect ratio, $h_w/l_w = 4.05$.
Wall thickness, $t_w = 12$ in. (305 mm).

Design Loads

Reinforced concrete structure self-weight.
Superimposed dead load = 30 psf (1.44 kPa).
Cladding = 550 lb per linear ft (8026 N/m) on building perimeter.
Parapet on roof = 550 lb per linear ft (8026 N/m) on building perimeter.
Floor live load = 50 psf (2.39 kPa).
Roof live load = 12 psf (0.57 kPa).
Building seismic weight = 4161 kips (18.5 MN) for first floor.
Building seismic weight = 3758 kips (16.7 MN) for roof.
Building seismic weight = 4085 kips (18.2 MN) for other floors.
Total building seismic weight:
$W_s = 4161 + (4)(4085) + 3758$
$= 24{,}259$ kips (107.9 MN)
Cumulative (from upper stories) wall unfactored design axial forces at base:
G_{dl} = 940 kips (4.18 MN) (due to unfactored design dead loads)
G_{ll} = 220 kips (0.98 MN) (due to unfactored unreduced design live loads)
Wall factored design axial force at base:
$N_{wd} = (1.0)(940) + (0.25)(220)$
$= 995$ kips (4.43 MN)

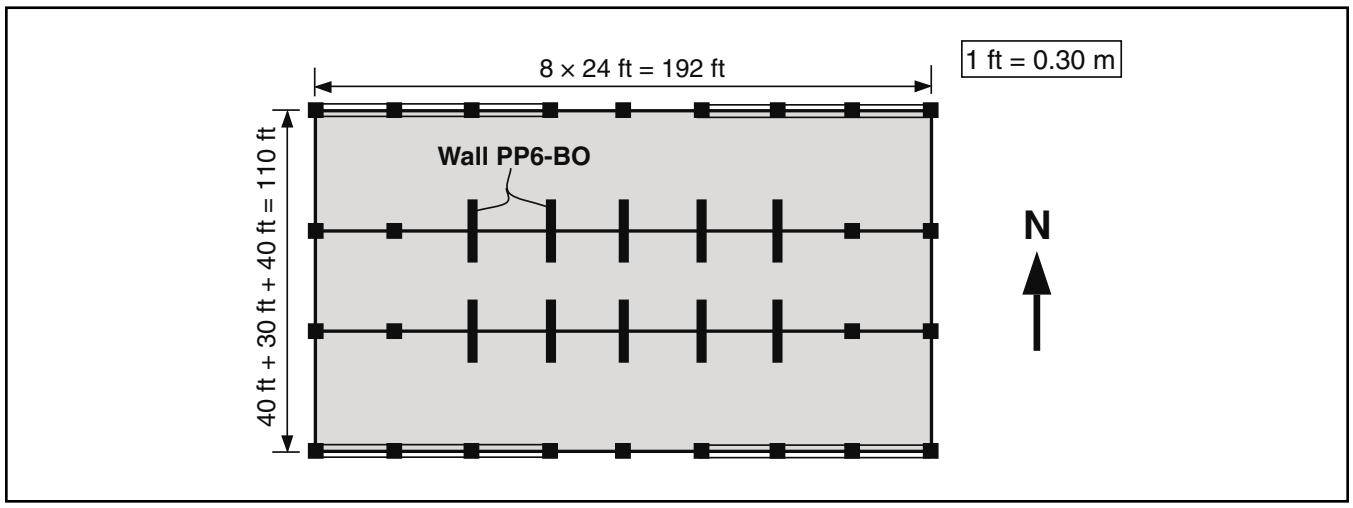

Fig. B1. Building plan.

Design Material Properties

Unconfined concrete compressive strength,
f'_c = 6 ksi (41.4 MPa).
Spiral steel yield strength, f_{spy} = 60 ksi (414 MPa)
Spiral steel strain at peak strength, ε_{spm} = 0.08
Mild flexural steel yield strength, f_{sy} = 60 ksi (414 MPa).
Mild flexural steel Young's modulus, E_s = 29,000 ksi (200 GPa).
Post-tensioning steel yield (i.e., linear limit) strength, f_{py} = 120 ksi (827 MPa).
Post-tensioning steel ultimate (i.e., peak) strength, f_{pu} = 160 ksi (1103 MPa).
Post-tensioning steel Young's modulus, E_p = 29,000 ksi (200 GPa).

Linear-Elastic Analysis Results for Lateral Load System (Ten Walls)

Modal analysis:
Linear-elastic first (i.e., fundamental) mode period, T_{e1} = 0.57 sec.
Structure effective linear-elastic first mode mass, M_{e1} = 43.1 kips-sec.^{2}/in. (7.55 kN-sec.^{2}/mm).
Resultant height of linear-elastic first mode inertia forces, H_v = 62.8 ft (19.1 m).
Lateral load analysis:
Structure linear-elastic lateral stiffness,
K_i = (10 walls) (369.7 kips/in./wall)
= 3697 kips/in. (647 kN/mm).

Strength Ratio, R_1

Assume roof displacement ductility ratio, μ_t = 10. Determine BP system regression coefficients corresponding to the seismic design conditions for this design example from Table 2 as:

a = 1.08
b = 0.89

Note that the regression coefficients for other selected seismic design conditions are also provided in Table 2. Then, from Eq. (4):

$$c = \frac{0.57^{1.08}}{0.57^{1.08} + 1} + \frac{0.89}{0.57} = 1.92$$

The strength ratio is calculated using Eq. (3) as:

$$R_1 = [1.92\,(10 - 1) + 1]^{1/1.92} = 4.54$$

Structure (Ten Walls) Design Base Shear Demand, V_{sd}

First, the site adjusted linear-elastic design spectral response acceleration, S is determined from IBC-2003.[19] Since the design is conducted for a seismic demand level of 2 percent probability of being exceeded in 50 years (corresponding to the Maximum Considered Earthquake in IBC-2003[19]), then:

$$S = S_{MS} \le \frac{S_{M1}}{T_{e1}}$$

where S_{MS} and S_{M1} are the Maximum Considered Earthquake spectral response accelerations for short periods and for 1-sec. period, respectively, calculated as:

$$S_{MS} = F_a S_s = (1.0)(2.05g) = 2.05g$$

and

$$S_{M1} = F_v S_1 = (1.5)(0.81g) = 1.22g$$

with F_a = 1.0 and F_v = 1.5 being the site coefficients determined from IBC-2003.[19]

$$\text{Since } \frac{S_{M1}}{T_{e1}} = \frac{1.22g}{0.57} = 2.14g > S_{MS} = 2.05g \quad \rightarrow \quad S = S_{MS} = 2.05g$$

The damping adjustment coefficient is calculated using Eq. (2). Assuming ξ = 3 percent and with ξ_0 = 5 percent:

$$f_\xi = \frac{[1 + (25)(0.05)]^{0.5}}{[1 + (25)(0.03)]^{0.5}} = 1.13$$

Then, the structure (ten walls) design base shear demand is calculated using Eq. (1) as:

$$V_{sd} = \frac{M_{e1} f_\xi S}{R_1}$$

$$= \frac{(43.1)(1.13)(2.05)(386.1)}{4.54}$$

$$= 8522 \text{ kips (37.9 MN)}$$

Wall Base Shear Force Demand, V_{wd}

The wall base shear force demand, V_{wd}, is determined by distributing the structure base shear demand, V_{sd}, vertically over the height and horizontally to the lateral load resisting members in the plan of the structure. Since only in-plane loads are considered and torsional effects are ignored, the wall base shear demand is:

$$V_{wd} = \frac{V_{sd}}{n_w} = \frac{8522}{10} = 852 \text{ kips (3.79 MN)}$$

Wall Nonlinear Roof Drift Demand, Δ_d

The wall nonlinear roof drift demand, Δ_d, is calculated using Eq. (5) as:

$$\Delta_d = \mu_t \frac{V_{wd}}{K_{wi}} \frac{100}{h_w}$$

$$= (10)\left(\frac{852}{3697/10}\right)\left(\frac{100}{(81)(12)}\right)$$

$$= 2.37 \text{ percent}$$

Since Δ_d = 2.37 percent is sufficiently close to the target roof drift of Δ_t = 2.4 percent, no iteration is needed on μ_t and the trial wall dimensions and number of walls in the structure are satisfactory.

Wall Base Moment Demand, M_{wd}

The wall base moment demand, M_{wd} is determined using the first mode distribution of inertia forces over the wall height as:

$$M_{wd} = V_{wd}H_v = (852)(62.8)$$

$$= 53{,}517 \text{ kip-ft } (72.6 \text{ MN-m})$$

Wall Flexural Reinforcement

The design of the wall flexural mild steel and post-tensioning steel reinforcement is based on a selected value of $\beta_m = 1.0$ for the mild steel moment ratio as described below.

Design of Post-Tensioning Steel Reinforcement

First, the design initial stress for the post-tensioning steel, f_{pi} is assumed. Let $f_{pi} = 0.55f_{pu} = (0.55)(160) = 88$ ksi (607 MPa). Then, an iterative procedure is executed as described below. Note that only the final step of the iteration is provided herein.

1. Assume a value for the length of the concrete rectangular compression stress block at the wall base as:

   $a_c = 57.5$ in. (1460 mm)

2. Determine the total area of the post-tensioning steel using Eq. (12) as:

$$A_p = \frac{2M_{wd}}{(\beta_m + 1)(l_w - a_c)f_{pi}} - \frac{N_{wd}}{f_{pi}}$$

$$= \frac{(2)(53{,}517)(12)}{(1 + 1)(240 - 57.5)(88)} - \frac{995}{88}$$

$$= 28.7 \text{ sq in. } (18{,}516 \text{ mm}^2)$$

3. Calculate the length of the concrete rectangular compression stress block using Eq. (13) as:

$$a_c = \frac{N_{wd} + A_p f_{pi}}{0.85 f'_c t_w}$$

$$= \frac{995 + (28.7)(88)}{(0.85)(6)(12)}$$

$$= 57.5 \text{ in. } (1460 \text{ mm})$$

4. Repeat Steps 1 to 3 until satisfactory agreement in the value of a_c is obtained (OK).

A total of nine pairs of 1⅜ in. (35 mm) diameter post-tensioning bars (with area of single bar, $a_p = 1.58$ sq in. (1019 mm^2) are selected [Fig. 2(a)]. The total area of post-tensioning steel provided in each wall is:

$$A_p = n_p a_p = (9)(2)(1.58) = 28.4 \text{ sq in. } (18{,}323 \text{ mm}^2)$$

which is acceptably close to the required steel area of $A_p = 28.7$ sq in. (18,516 mm^2) (OK).

Design of Mild Steel Reinforcement

The required mild steel area, A_s to satisfy the wall design base moment demand is determined using an iterative procedure as follows. Note that only the final step of the iteration is provided herein.

Assume that the distance from the compression end of the wall to the centroid of A'_s is equal to $d'_{sc} = 13.25$ in. (337 mm) Then, using Eq. (15):

$$A_s = \frac{M_{wd}\beta_m}{(\beta_m + 1)(l_w - 2d'_{sc})f_{sy}}$$

$$= \frac{(53{,}517)(12)(1)}{(1 + 1)[240 - (2)(13.25)](60)}$$

$$= 25.1 \text{ sq in. } (16{,}194 \text{ mm}^2)$$

A total of 10 pairs of No. 10 bars are used on each side of the wall [Fig. 2(a)], resulting in a steel area of:

$$A_s = A'_s = (10)(2)(1.27) = 25.4 \text{ sq in. } (16{,}387 \text{ mm}^2)$$

The bars are spaced 2.5 in. (64 mm) apart with a concrete cover of 2 in. (51 mm), resulting in $d'_{sc} = 13.25$ in. (337 mm) as assumed (OK).

Once the mild steel bars are selected and placed in the cross section, the strains in the bars are calculated assuming a linear strain diagram (i.e., plane sections assumption). If the calculated bar strains are smaller than the yield strain, then, the determination of A_s above may need to be revised using a modified form of Eq. (9).

The neutral axis depth at the base of the wall is calculated as:

$$c_c = \frac{a_c}{\beta_1} = \frac{57.5}{0.75} = 76.7 \text{ in. } (1948 \text{ mm})$$

Assuming a concrete cover of 2 in. (51 mm), the distance of the innermost compression-side bar from the compression end of the wall is:

$$d'_{si} = 2 + (9)(2.5) = 24.5 \text{ in. } (622 \text{ mm})$$

The strain in the bar is calculated assuming an extreme concrete compression strain of 0.003:

$$\varepsilon'_{si} = \frac{c_c - d'_{si}}{c_c}(0.003)$$

$$= \left(\frac{76.7 - 24.5}{76.7}\right)(0.003)$$

$$= 0.00204 \rightarrow \text{at yield (OK)}$$

Similarly, the distance of the innermost tension-side bar from the compression end of the wall is:

$$d_{si} = 240 - 2 - (9)(2.5) = 215.5 \text{ in. } (5474 \text{ mm})$$

The strain in the bar is:

$$\varepsilon_{si} = \frac{d_{si} - c_c}{c_c}(0.003)$$

$$= \left(\frac{215.5 - 76.7}{76.7}\right)(0.003)$$

$$= 0.00543 \rightarrow \text{above yield (OK)}$$

Concrete Confinement

Concrete confinement is needed at the wall boundaries to prevent premature crushing and failure of the concrete before the wall roof drift demand, Δ_d is reached. As described in the main body of the paper, this requires an iterative procedure. Only the final step of the iteration is provided herein.

A confinement model developed by Mander et al.,[21] is used to develop the stress-strain relationship of the confined concrete as shown in Fig. B2. For spiral confinement properties of spiral center-to-center diameter, D_{sp} = 10.3 in. (262 mm), spiral wire diameter, d_{sp} = 0.356 in. (9 mm), and spiral pitch, s_{sp} = 1.50 in. (38 mm) (resulting in a spiral reinforcement ratio, ϱ_{sp} = 2.57 percent), the following confined concrete stress-strain relationship parameters are determined:

– Compressive strength of confined concrete, f'_{cc} = 9.97 ksi (69 MPa); and
– Ultimate (crushing) strain of confined concrete, ε_{cu} = 0.0213

Then, the neutral axis depth corresponding to the crushing of the confined concrete at the wall base is estimated using Eq. (17) as:

$$c_{cu} = \frac{N_{wd} + A_p f_{py}}{0.85 f'_{cc} t_w}$$

$$= \frac{995 + (28.44)(120)}{(0.85)(9.97)(12)}$$

$$= 43.3 \text{ in. (1100 mm)}$$

It is assumed that all of the post-tensioning bars in the wall are at the yield stress. The corresponding curvature ϕ_{cu} at the wall base is estimated by assuming that the wall lateral displacements occur as a result of a concentrated rotation at the wall base and that the flexural deformations are uniformly distributed over a "plastic hinge height" using Eq. (18) as:

$$\phi_{cu} = \frac{\Delta_d}{0.2 l_w} = \frac{0.0237}{(0.2)(240)} = 0.000494$$

where $0.2l_w$ is the assumed plastic hinge height. Finally, the required strain capacity of the confined concrete, ε_{cu}, is determined from Eq. (16) as:

$$\varepsilon_{cu} = c_{cu} \phi_{cu} = (43.3)(0.000494) = 0.0214$$

Since the ultimate strain capacity, ε_{cu} = 0.0213 is sufficiently close to the demand, ε_{cu} = 0.0214, the design of the concrete confinement reinforcement is satisfied.

The confinement reinforcement should extend over a length, l_c, and height, h_c, near both ends of the wall at the base where the concrete strains are greater than or equal to ε_u = 0.004, which is the assumed crushing strain of the unconfined concrete. A linear strain diagram defined by ϕ_{cu} and c_{cu} is used to determine the confined wall length at each end, resulting in:

$$l_c = c_{cu}\left(1 - \frac{\varepsilon_u}{\varepsilon_{cu}}\right)$$

$$= (43.3)\left(1 - \frac{0.004}{0.0214}\right)$$

$$= 35.2 \text{ in. (894 mm)}$$

The determination of the confined wall height, h_c, depends on the bending moment diagram over the wall height and is not within the scope of this example.

Detailing of Mild Steel Reinforcement

Fracturing of the mild steel reinforcement should be prevented. For this purpose, a linear strain diagram defined by ϕ_{cu} and c_{cu} is used to estimate the maximum strain, ε_{sm}, in the mild steel bar on the extreme tension side of the wall. The distance of the outermost tension-side bar from the compression end of the wall is:

$$d_{so} = 240 - 2 = 238 \text{ in. (6045 mm)}$$

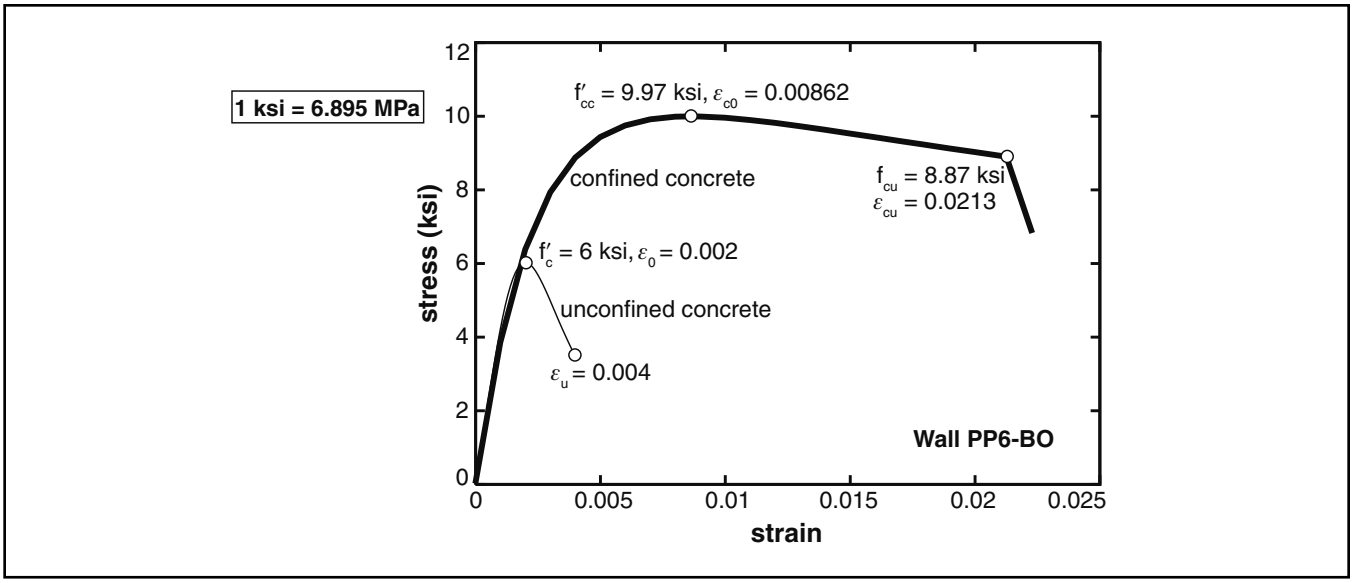

Fig. B2. Confined and unconfined concrete stress-strain relationships for Wall PP6-BO.

The strain in the bar is:

$$\varepsilon_{sm} = \frac{d_{so} - c_{cu}}{c_{cu}} \varepsilon_{cu}$$

$$= \left(\frac{238 - 43.3}{43.3}\right)(0.0214)$$

$$= 0.0962 \rightarrow \text{below fracture strain (OK)}$$

If necessary (e.g., due to low cycle fatigue failure concerns), the strains in the mild steel reinforcement can be reduced by placing the bars closer to the wall centerline (which may require a redesign) and/or by wrapping the bars to prevent bond over a predetermined height above the base-panel-to-foundation joint. Determination of the wrapped length of mild steel reinforcement is not discussed in this paper.

The mild steel reinforcement should be properly anchored to the foundation and should be extended to a sufficient height above the base of the wall to allow for the development of the ultimate (i.e., peak) strength of the steel in tension and compression at the base-panel-to-foundation joint. The bars that are no longer needed for flexural resistance may be terminated (i.e., cut off) in a staggered pattern over the wall height. The detailing of the mild steel bars over the wall height is not addressed in this design example.

Yielding of Post-Tensioning Steel Reinforcement

First, the additional elongation, u_{py}, of the post-tensioning steel from f_{pi} to f_{py} is estimated from Eq. (22):

$$u_{py} = \frac{f_{py} - f_{pi}}{E_p} l_{pu}$$

$$= \left(\frac{120 - 88}{29{,}000}\right)(81)(12)$$

$$= 1.07 \text{ in. } (27 \text{ mm})$$

where the unbonded length of the post-tensioning steel, l_{pu}, is equal to the wall height, h_w.

The distance, d_{py}, of the post-tensioning bar with the largest strain from the compression end of the wall is:

$$d_{py} = 120 + (0.5)(8)(5) = 140 \text{ in. } (3556 \text{ mm})$$

Since the yielding of the post-tensioning steel in Wall PP6-BO is expected to occur significantly before the crushing of the confined concrete, the neutral axis depth corresponding to the yielding of the post-tensioning steel, c_{py}, is assumed to be equal to:

$$c_{py} = \frac{c_{cu}}{0.75} = \frac{43.3}{0.75} = 57.8 \text{ in. } (1468 \text{ mm})$$

Then, the roof drift corresponding to the yielding of the post-tensioning steel is estimated from Eq. (21) as:

$$\Delta_{py} = \frac{u_{py}}{d_{py} - c_{py}}$$

$$= \left(\frac{1.07}{140 - 57.8}\right)(100)$$

$$= 1.30 \text{ percent}$$

Note that the prevention of the yielding of the post-tensioning steel is not a design performance objective for Wall PP6-BO. If the yielding of the post-tensioning steel needs to be delayed, a new (lower) value of f_{pi} should be used in Eqs. (12) and (13) and/or the tendons should be placed closer to the wall centerline, and the design should be repeated.

Shear Design

Shear design of the wall to prevent diagonal tension failure of the wall panels, shear slip failure along the horizontal joints, and failure along the bottom and top edges of the base panel is not within the scope of this design example.

Stability of Wall Panels

Design to prevent out-of-plane buckling of the wall panels between lateral restraints (usually at the floor and roof levels) and to prevent buckling of the compression zone in the base panel is not within the scope of this example.

Comparisons with Static Lateral Load Analysis Results

Fig. 6(a) shows the base shear versus roof drift (V-Δ) behavior obtained from a nonlinear static monotonic analysis of Wall PP6-BO. The limit states from the analysis results are compared with the design estimations as follows.

1. Yielding of mild steel at centroid of bar group on tension side of wall—The analysis results indicate that this limit state is reached at a base shear of $V = 853$ kips (3.79 MN), which satisfies the wall design base shear demand of $V_{wd} = 852$ kips (3.79 MN) → wall lateral strength (OK).
2. Crushing of confined concrete at wall base—The analysis results indicate that this limit state is reached at a roof drift of $\Delta = 2.40$ percent, which satisfies the wall design nonlinear roof drift demand of $\Delta_d = 2.37$ percent → wall lateral displacement capacity (OK).
3. Yielding of post-tensioning steel—The analysis results indicate that this limit state is reached at a roof drift of $\Delta = 1.38$ percent, which agrees reasonably well with the design estimation of $\Delta_{py} = 1.30$ percent. Note that this is not a design requirement for Wall PP6-BO.